DESIGN OF A METAL VIBRATION ISOLATOR WITH HIGH INTERNAL DAMPING

A THESIS SUBMITTED TO
THE GRADUATE SCHOOL OF NATURAL AND APPLIED SCIENCES
OF
MIDDLE EAST TECHNICAL UNIVERSITY

BY

MUHAMMED ENES İSANÇ

IN PARTIAL FULFILLMENT OF THE REQUIREMENTS
FOR
THE DEGREE OF MASTER OF SCIENCE
IN
MECHANICAL ENGINEERING

DECEMBER 2023

Approval of the thesis:

DESIGN OF A METAL VIBRATION ISOLATOR WITH HIGH INTERNAL DAMPING

submitted by **MUHAMMED ENES İSANÇ** in partial fulfillment of the requirements for the degree of **Master of Science** i**n Mechanical Engineering, Middle East Technical University** by,

Prof. Dr. Halil Kalıpçılar
Dean, Graduate School of **Natural and Applied Sciences** _____

Prof. Dr. M. A. Sahir Arıkan
Head of the Department, **Mechanical Engineering** _____

Assist. Prof. Dr. Gökhan O. Özgen
Supervisor, **Mechanical Engineering, METU** _____

Examining Committee Members:

Prof. Dr. Yiğit Yazıcıoğlu
Mechanical Engineering, METU _____

Assist. Prof. Dr. Gökhan O. Özgen
Mechanical Engineering, METU _____

Prof. Dr. Ender Ciğeroğlu
Mechanical Engineering, METU _____

Assist. Prof. Dr. Orkun Özşahin
Mechanical Engineering, METU _____

Assoc. Prof. Dr. Reza Aghazadeh
Aeronautical Engineering, THK Uni. _____

Date: 06.12.2023

I hereby declare that all information in this document has been obtained and presented in accordance with academic rules and ethical conduct. I also declare that, as required by these rules and conduct, I have fully cited and referenced all material and results that are not original to this work.

Name Last name : Muhammed Enes İsanç

Signature :

ABSTRACT

DESIGN OF A METAL VIBRATION ISOLATOR WITH HIGH INTERNAL DAMPING

İsanç, Muhammed Enes
Master of Science, Mechanical Engineering
Supervisor : Assist. Prof. Dr. Gökhan O. Özgen

December 2023, 77 pages

Metal vibration isolators are significant in terms of isolating the vibration and shocks in the systems which require high damping isolation. This thesis study has two primary objectives. The first objective is to enhance the vibration isolation performance of previously designed passive metal vibration isolators for space launch vehicle, which exhibit high transmissibility values at high frequencies, by increasing their internal damping. The second objective is to estimate the fatigue life of the designed vibration isolators both including previously designed triple test configuration and the new concept design.

The concept of adding a tuned vibration absorbers (TVAs) to the previously designed triple test structure is explored. TVAs parameters are defined, and a parametric optimization study is conducted to demonstrate the applicability of TVAs. Subsequently, the vibration isolation system is addressed, and a TVA design tailored to the identified target mode is developed. Finally, effect of TVA usage is verified by finite element analyses in ABAQUS software and vibration tests in a laboratory environment.

The fatigue life estimation has performed by using ANSYS software fatigue tool. After doing modal analysis and random vibration response analysis, the fatigue life

has measured with ANSYS fatigue life measurement feature. The obtained results show that design has enough life expentancy value in terms of fatigue.

Keywords: Metal Vibration Isolators, High Damping Concepts, Fatigue Life Estimation, Finite Element Analysis, Tuned Vibration Absorbers

ÖZ

YÜKSEK İÇ SÖNÜMLEMELİ METAL TİTREŞİM İZOLATÖRÜ TASARIMI

İsanç, Muhammed Enes
Yüksek Lisans, Makina Mühendisliği
Tez Yöneticisi: Dr. Öğr. Üyesi Gökhan O. Özgen

Aralık 2023, 77 sayfa

Yüksek sönümlemeli izolasyon gerektiren sistemlerin, titreşim ve şoklara karşı izole edilmesi açısından metal titreşim izolatörleri, öneme sahiptir. Bu tez çalışmasının iki temel amacı bulunmaktadır. İlk hedef, daha önce uzay fırlatma aracı için tasarlanmış pasif metal titreşim izolatörlerinin içsel sönümlemelerini artırarak. titreşim izolasyon performanslarını artırmaktır. Bu izolatörler yüksek frekansta yüksek geçirgenlik değerlerine sahiptir. İkinci hedef, daha önce tasarlanmış üçlü test konfigürasyonuna ait ve yeni konsept tasarımdaki titreşim izolatörlerinin yorgunluk ömrünü tahmin etmektir.

Ayarlı titreşim emici (TVA) kullanımı konsepti, daha önce tasarlanmış üölü test yapısı üzerinde incelenmiştir. TVA'ların parametreleri tanımlanmış ve uygulanabilirliklerini göstermek amacıyla parametrik bir optimizasyon çalışması yapılmıştır. Daha sonra titreşim izolasyon sistemi ele alınmış ve belirlenen hedef moda uygun bir TVA tasarımı geliştirilmiştir. Son olarak, TVA kullanımının etkisi, ABAQUS yazılımında yapılan sonlu eleman analizleri ve laboratuvar ortamında gerçekleştirilen titreşim testleri ile doğrulanmıştır.

Yorulma ömrü tahmini, ANSYS yazılımı yorulma aracı kullanılarak yapılmıştır. Modal analiz ve rastgele titreşim tepki analizi yapıldıktan sonra ANSYS yorulma

ömrü ölçüm özelliği ile yorulma ömrü ölçülmüştür. Elde edilen sonuçlar tasarımın yorulma açısından yeterli ömür değerine sahip olduğunu göstermektedir.

Anahtar Kelimeler: Metal Titreşim İzolatörleri, Yüksek Sönümleme Konseptleri, Yorulma Ömrü Kestirimi, Sonlu Elemanlar Analizi, Ayarlı Titreşim Emiciler

To My Precious Family

ACKNOWLEDGMENTS

I would like to thank my esteemed thesis advisor Assist. Prof. Dr. Gökhan O. Özgen for his contributions to me during the design development and improvement phase and finally for his dedication and positive approach for the good execution of the process.

I would like to thank Mr. Alper ATAK for his assistance in the manufacturing of the test components.

I would like to express my gratitude to Mr. Onur ÖZGELEN for his technical support in conducting the tests.

I would like to thank everyone who gave me motivation to present my thesis successfully.

TABLE OF CONTENTS

ABSTRACT v

ÖZ vii

ACKNOWLEDGMENTS x

TABLE OF CONTENTS xi

LIST OF TABLES xiii

LIST OF FIGURES xv

LIST OF ABBREVIATIONS xviii

CHAPTERS

1 INTRODUCTION 1

2 LITERATURE REVIEW 3

2.1 Damping Improvement Concepts 3

2.2 Fatigue Life Estimation Methods 9

3 CONCEPT DEVELOPMENT 13

3.1 About Previous Study 13

3.2 TVA Applicability Demonstration 18

3.2.1 Axial TVA Implementation 22

3.2.2 Lateral TVA Implementation 30

3.2.3 Both Axial and Lateral TVA Implementation 32

3.3 Target Mode Determination 39

4 PROOF OF CONCEPT 49

4.1 TVA Design Theoretically 49

4.2 TVA Design Physically 51

4.3 Test Procedure 56
5 FATIGUE LIFE ESTIMATION 63
6 CONCLUSION 73
REFERENCES 75

LIST OF TABLES

TABLES

Table 3.1 Resonance Frequencies of Triple Test Structure 21
Table 3.2 Resonance Frequencies of Triple Test Structure in Axial Direction 22
Table 3.3 TVA Parameters for 1800 Hz 24
Table 3.4 TVA Parametric Results for 1800 Hz in Axial Direction 26
Table 3.5 Transmissibility Comparison of Without TVA and P2 in Axial Direction 26
Table 3.6 TVA Parameters for 1335 Hz 28
Table 3.7 Double TVA Parametric Results in Axial Direction 28
Table 3.8 Transmissibility Comparison of Without TVA, P2, P2+P8 and P8 in Axial Direction 29
Table 3.9 Resonance Frequencies of Triple Test Structure in Lateral Direction 30
Table 3.10 TVA Parameters for 1338 Hz 32
Table 3.11 Transmissibility Comparison of Without TVA, P10, P11 and P12 in Lateral Direction 32
Table 3.12 Transmissibility Comparison of Without TVA and P8+P10 in Axial Direction 33
Table 3.13 Transmissibility Comparison of Without TVA and P8+P10 in Lateral Direction 34
Table 3.14 TVA Parameters for 1097.5 Hz 35
Table 3.15 Triple TVA Parametric Results in Lateral Direction 35
Table 3.16 Transmissibility Comparison of Without TVA, P8+P10, P8+P10+P16 and P8+P16 in Lateral Direction 36
Table 3.17 Double TVA Parametric Results in Lateral Direction 37
Table 3.18 Transmissibility Comparison of Without TVA and with Double TVA in Axial Direction 38
Table 3.19 Transmissibility Comparison of Without TVA and with Double TVA in Lateral Direction 39

Table 4.1 TVA Parameters for 1389 Hz.....50

LIST OF FIGURES

FIGURES

Figure 2.1 Fatigue Life Estimation Procedure Diagram [24] 10
Figure 3.1 Schematic of Vibration Isolation System for Space Launch Vehicle [26] 14
Figure 3.2 Vibration Isolator Damping Concept, S1 [26] 15
Figure 3.3 Vibration Isolator Damping Concept, T1 [26] 15
Figure 3.4 Vibration Isolator Damping Concept, T2 [26] 15
Figure 3.5 Vibration Isolation System Consisting of 60 Isolators 16
Figure 3.6 Test Setup of T1 [26] 16
Figure 3.7 The comparison of axial transmissibility curves obtained from sine sweep test and finite element analysis for upper point [26] 17
Figure 3.8 The comparison of lateral transmissibility curves obtained from sine sweep test and finite element analysis for upper point [26] 17
Figure 3.9 Axial TVA representation 19
Figure 3.10 Lateral TVA Representation 19
Figure 3.11 Nomograph of Viscoelastic Damping Polymer 112 Series [27] 20
Figure 3.12 Internal Resonance of Isolator, 1338 Hz 21
Figure 3.13 Internal Resonance of Isolator, 1380 Hz 22
Figure 3.14 Transmissibility Plot in Axial Direction Without TVA Implementation 23
Figure 3.15 Location of TVA Tuned at 1800 Hz 23
Figure 3.16 Kinematic Coupling of Mass-Spring-Dashpot System 25
Figure 3.17 Continuum Distributing Coupling of Mass-Spring-Dashpot System .. 26
Figure 3.18 Location of TVAs Tuned at 1335 and 1800 Hz 27
Figure 3.19 Transmissibility Comparison Plot in Axial Direction for TVA Applied Only Upper Surface at 1335 Hz 30
Figure 3.20 Transmissibility Plot in Lateral Direction Without TVA Implementation 31

Figure 3.21 Location of TVA Tuned at 1338 Hz 31
Figure 3.22 Location of TVA Tuned at 1335 Hz and 1338 Hz 33
Figure 3.23 Location of TVA Tuned at 1335 Hz, 1338 Hz and 1097.5 Hz 34
Figure 3.24 Location of TVA Tuned at 1335 Hz and 1097.5 Hz 36
Figure 3.25 Transmissibility Comparison Plot for Double TVA in Axial Direction 38
Figure 3.26 Transmissibility Comparison Plot for Double TVA in Lateral Direction 39
Figure 3.27 Rocking Mode Shape of Isolation System, 14 Hz 40
Figure 3.28 Torsional Mode Shape of Isolation System, 18 Hz 41
Figure 3.29 Lateral Mode Shape of Isolation System, 62 Hz 41
Figure 3.30 Axial Mode Shape of Isolation System, 83 Hz 42
Figure 3.31 Internal Resonance of Isolators, 1479 Hz 42
Figure 3.32 Internal Resonance of Isolators, 1693 Hz 43
Figure 3.33 Transmissibility Plot in Axial Direction for Isolation System 44
Figure 3.34 Transmissibility Plot in Lateral Direction for Isolation System 44
Figure 3.35 Rocking Mode Shape of Quadruple Test Configuration, 62 Hz 46
Figure 3.36 Axial Mode Shape of Quadruple Test Configuration, 137 Hz 46
Figure 3.37 Torsional Mode Shape of Quadruple Test Configuration, 153 Hz 47
Figure 3.38 Lateral Mode Shape of Quadruple Test Configuration, 231 Hz 47
Figure 3.39 Internal Resonances of Isolators: 1389 Hz, 1410 Hz, 1440 Hz 48
Figure 3.40 Transmissibility Plot in Lateral Direction for Quadruple Test Configuration 48
Figure 4.1 Location of TVA Tuned at 1389 Hz 49
Figure 4.2 Parametric Transmissibility Comparison of TVAs Tuned at 1389 Hz 51
Figure 4.3 Nomogram of 3M-468 MP [28] 52
Figure 4.4 Material Definition of 3M-468 MP in ANSYS 53
Figure 4.5 Geometrical Representation of TVA 53
Figure 4.6 Schematic of TVA 54
Figure 4.7 Direct Point FRF at the Tip Point of TVA 54

Figure 4.8 Quadruple Test Configuration with TVAs 55
Figure 4.9 Transmissibility Comparison Plot in Lateral Direction for Quadruple Test Configuration 56
Figure 4.10 TVA Tuned at 1400 Hz 57
Figure 4.11 Vibration Environment of Minotaur-Payload During Launch [29]..... 58
Figure 4.12 General View of Quadruple Test Structure Without TVA..... 58
Figure 4.13 Experimental Setup for Vibration Testing 59
Figure 4.14 General View of One Isolator With TVA 59
Figure 4.15 General View of Quadruple Test Structure With TVAs 60
Figure 4.16 Random Vibration Test Comparison Plot in logx-logy Scale 61
Figure 4.17 Random Vibration Test Comparison Plot in x-logy Scale 61
Figure 4.18 Response PSD Comparison Plot in x-logy Scale 62
Figure 5.1 General View of Previous Triple Test Configuration 63
Figure 5.2 Material Properties of ISD112 Polymer 64
Figure 5.3 Meshing of Triple Test Stucture Assembly..... 64
Figure 5.4 Equivalent Stress Results of Triple Test Stucture for Axial PSD Input 65
Figure 5.5 Fatigue Life Expactation of Triple Test Stucture for Axial PSD Input. 66
Figure 5.6 Equivalent Stress Results of Triple Test Stucture for Lateral PSD Input 67
Figure 5.7 Fatigue Life Expactation of Triple Test Stucture for Lateral PSD Input 67
Figure 5.8 Meshing of Quadruple Test Stucture Assembly..... 68
Figure 5.9 Fatigue Life Expactation of Quadruple Test Stucture Without TVAs for Lateral PSD Input 69
Figure 5.10 Fatigue Life Expactation of Quadruple Test Stucture With TVAs for Lateral PSD Input 69
Figure 5.11 Equivalent Stress Results of Isolators Without VEM Layers for Axial PSD Input..... 70
Figure 5.12 Equivalent Stress Results of Isolators Without VEM Layers for Lateral PSD Input..... 71

LIST OF ABBREVIATIONS

ABBREVIATIONS

PAF Payload attach fitting

VEM Viscoelastic material

MRE Magneto-rheological elastomer

LVI-ECD Lever-type vibration isolator with eddy current damping

QZS Quasi-zero stiffness

LRELS Lead-rubber elliptical leaf spring

WSVI Whole-spacecraft vibration isolator

PLA Polylactide

PSD Power spectral density

BC Boundary Condition

TVA Tuned Vibration Absorber

FRF Frequency Response Function

FEA Finite Element Analysis

CHAPTER 1

INTRODUCTION

Successful spacecraft launches demand careful consideration of their resilience to the challenges posed by the launch environment. Structure-borne vibrations and acoustic excitation, transmitted through the payload attach fitting (PAF), significantly influence spacecraft performance during this phase. Passive whole-spacecraft vibration isolation systems have been developed to significantly reduce dynamic launch loads. The most known designs are a single-axis SoftRide axial system for axial loads and a multi-axis system for Minotaur vehicle's dynamic loads. The multi-axis SoftRide system introduces flexibility and damping in three orthogonal axes, effectively mitigating both axial and lateral dynamic launch loads. Successful flight missions, such as Minotaur/JAWSAT and Minotaur/MightySat, validate the system's efficiency in reducing dynamic launch loads [1].

The motivation for this thesis study is to improve internal damping of the previously designed passive vibration isolation system for spacecraft launch system, to estimate fatigue life of a designed passive metal vibration isolator. Increasing internal damping of the metal isolators around resonance frequencies results in improvement on vibrational performance. It is essential to explore the importance of isolating PAF vibrations by improving the damping capability of metal based vibration isolator without getting any failure. Therefore, the fatigue life estimation is required for both failure concept and planning replacement time for the vibration isolation system. The thesis consists of four main parts with the light of explained objective.

In the first main part of the thesis, an extensive literature review was conducted on the subject, encompassing research on both damping enhancement methods and fatigue life prediction methods.

In the second main part of the thesis, a brief summary of the previously conducted thesis, highlighting its areas of improvement, and establishing its context with this thesis has been provided. Moreover, it has been tried to reveal that TVA application is suitable for diminishing the peak value of transmissibility at a specific resonance frequency. Then, problematic mode shape and resonance frequency of the isolation system has been found.

In the third main part of the thesis, improving and getting high internal damping for the vibration system by using TVA has been proven with both using FEA software and conducting experiment.

In the fourth main part of the thesis, random vibration fatigue analysis is performed to reveal the fatigue life of the vibration isolation system. During fatigue analysis, ANSYS sofware fatigue tool is used to compare the estimated life values of pre-designed failured part and the new design.

Finally, the thesis work is summarized as a whole, including shortcomings, challenges and possible improvements.

CHAPTER 2

LITERATURE REVIEW

2.1 Damping Improvement Concepts

There are numereous study about designing vibration isolator by getting high damping capability and vibration suppression performance in the literature. Some of them are explained in this section.

The research on Magneto-rheological elastomers (MREs) has been highly regarded for developing active vibration isolators and shock absorbers thanks to their modifiable damping characteristics and stiffness. Conventional MRE-based isolators have been effective in diminishing undesirable structural and machinery vibrations by enhancing stiffness through the MR effect when the magnetic field is intensified. However, Yang, Sun, Du, Li, Alici and Deng have presented a novel MRE isolator with reduced stiffness as the applied current is increased [2]. They accomplished this by employing a hybrid magnet, which incorporates both an electromagnet and permanent magnets, within a multilayered MRE structure.

Yan, Wang, Ma, Bao, Wang and Wu have introduced a lever-type vibration isolator with eddy current damping (LVI-ECD) to extend the range of isolation capabilities and enhance vibration suppression [3]. It utilizes a lever with a permanent magnet at its tip, inducing eddy current damping between the permanent magnet and conductive base and load plates. The lever structure amplifies the damping effect, resulting in improved performance, especially in resonant frequencies. They analyzed various parameters for their effects on vibration isolation by experiments to confirm the effectiveness of the LVI-ECD.

Wu, Chen and Shan utilized a negative stiffness effect in a vibration isolator by employing three magnets in parallel [4]. Two of these magnets were fixed, while the

third one was positioned in the middle, allowing for up and down movement. This configuration resulted in high static and low dynamic stiffness. To ensure consistency in their experiments, a coil spring was used at the bottom. The negative stiffness effect was produced by the movement of the magnets. While low stiffness values showed linearity in the experiments, higher frequencies displayed nonlinearity.

For numerous practical applications, such as space equipment and aviation crafts, the volume and weight of quasi-zero stiffness (QZS) vibration isolators become impractical. However, Li, Wu and Jiang have achieved a simple structural form and lightweightness in the vibration isolator design by employing bistable laminates [5].

Yilmaz and Kikuchi have developed a stiff passive vibration isolator, which has low weight, with a broad stopband at low frequencies [6]. They formulated bandwidths for dynamic vibration absorbers with a single degree of freedom and anti-resonant vibration isolators employing a lever-type configuration. Using these formulations, a two degree of freedom vibration isolator has synthesized to achieve a substantial bandwidth at low frequencies, benefitting from inertial coupling and asymmetry in the inertial forcing terms.

Leblouba, Altoubat, Ekhlasur Rahman and Palani Selvaraj have added the lead-rubber elliptical leaf spring (LRELS) to improve the damping and energy dissipation characteristics of the current elliptical leaf spring through enhancements. [7]. LRELS exhibits nonlinear hysteretic behavior, with symmetrical rate-independent characteristics in ground plane but asymmetric behavior in the normal plane. Mathematical models based on the Bouc-Wen model have been developed and verified through finite element analyses. LRELS demonstrates effectiveness in both in-plane and vertical directions, attributed to the enhanced damping from the lead spring's hysteretic behavior in their work.

Tang, Cao, Qin, Li and Chen have presented a novel whole-spacecraft vibration isolator (WSVI) comprising supporting leaf springs, voice coil motors, and actuator supports to mitigate structural vibrations during spacecraft launch [8]. The device

features a compact and lightweight design, meeting vibration isolation requirements without altering the PAF structure. A dynamic model has been established by them to evaluate the WSVI's performance under external excitations. Results show that the novel WSVI effectively reduces spacecraft vibration amplitudes and significantly mitigates vibrations during launch.

Kim and Kang have designed a novel band-stop filter-type vibration isolator with a lever structure inspired by the V-shaped configuration in the human middle ear [9]. The designed isolator allows higher geometric freedom in mechanical design and enables tuning of anti-resonance frequencies by adjusting parameters such as mass ratios and lever dimensions.

Pierrick, Ohayon and Le Bihan have presented preliminary results on semi-active vibration isolation using MR dampers during spacecraft launch [10]. Their study includes single degree of freedom and soft hexapod configurations. Semi-active isolation outperforms passive isolation for broadband disturbance with MR dampers and a clipped-continuous skyhook control scheme.

Johnson and Ruzzene have worked on the potential benefits of resonance-based metamaterials for passive vibration control in heavy machinery [11]. Practical implementation in industrial applications has been limited due to space constraints and high static stiffness requirements. Several resonance-based concepts were analyzed as candidates for retrofitting or replacing elastic supports in large generators. Grounded resonators and targeted rotational modes were used to reduce vibration at specific frequencies. The results show successful reduction of off-resonance operating frequencies, demonstrating the effectiveness of resonance-based metamaterials in reducing vibration transmission in massive machinery.

Park, Kwon, Koo and Oh’s study focuses on developing a three-axis passive launch-vibration isolation system for small satellites, using superelastic shape memory alloy technology [12]. Their goal is to reduce design-load and vibration-test specifications for on-board components, resulting in more efficient, expedited, cost-effective, and lightweight satellite development. The proposed system utilizes superelastic shape

memory alloy blades with viscous lamina adhesive layers of acrylic tape for superior damping characteristics. They conducted static load tests to obtain the system's basic characteristics with varying numbers of viscoelastic multilayers. The efficacy of the design was further verified through launch environment simulations involving sine and random vibration tests performed by them.

Dunaj, Berczyński, Miądlicki, Irska and Niesterowicz conducted a study on passive vibration elimination by applying low dynamic stiffness elements to cover structural components using polylactide (PLA) [13]. The PLA cover was created using 3D printing technology and connected to the structure through a press connection. The arrangement of the PLA cover was found to significantly enhance the dissipation properties of the structure. The research presents analyses that involve varying and studying different parameters of how the thickness and distribution of the PLA cover impact the increase in the structure's dissipation properties.

The SoftRide OmniFlex is a multi-axis, low-profile vibration isolation mount renowned for its high passive damping capabilities [14]. It offers independently ascertainable flexibility in all vibrational directions, with lateral compliance achieved through the flexure loop section. The OmniFlex's superior passive damping is achieved through the VEM layer affixed to both the lower and upper flexure segments, inducing significant shear stress during relative translational motion. These vibration isolators are strategically placed between payload adapter and the spacecraft [14].

Turker, Cigeroglu and Ozgen have been worked on designing vibration test fixture [15]. They designed TVA’s to diminish peaks at fixture's local resonances because existence of them would result in resonant vibration behavior, which occasionally would make it impossible for the shaker control system to provide the intended random vibration profile. They obtained better vibrational suppression performance by using TVA’s at these local frequencies.

Mrabet, Ichchou, and Bouhaddi concentrated on mitigating the interior sound pressure resulting from the random vibrations of structures connected to an air-filled

enclosure [16]. They utilized a tuned mass damper for controlling low-frequency vibrations. To enhance the performance of the tuned mass damper, a stochastic acoustic optimization approach is suggested. The objective function in this approach is the root mean square acoustic pressure measured at a specific location within the enclosure. The results indicate that when plate modes dominate the desired modes, employing broad-spectrum control is effective, leading to significant reductions in power spectral density responses. This effect is particularly evident with a relatively high mass ratio for the tuned mass damper devices.

Gardonio and Zilletti conducted a simulation study on two integrated TVAs designed to effectively control the global flexural oscillation of lightly damped thin structures exposed to disturbances across a wide frequency spectrum [17]. The first TVA uses a single axial switching configuration, where a seismic mass is installed on variable damping components and axial spring. This allows for iterative switching of characteristic damping and natural frequency, providing control over the resonant response of three flexural modes within the hosting structure. The second TVA adopts a single three-axes configuration, incorporating a seismic mass installed on dampers and axial and rotational springs, allowing for independent heave and pitch-rolling vibrations. Results from the simulation study show that the proposed single-unit absorbers achieve reductions of 5.3 dB and 8.7 dB, respectively, in the overall flexural vibration of a rectangular plate within the 20-120 Hz frequency range.

Iglesias, Aguirre, Munoa, Dombovari, Laka, and Stepan explored the development of a prototype for a self-tuning vibration absorber with variable stiffness. Additionally, they formulated a novel tuning function to minimize the response at the frequency corresponding to the wheel's rotational speed [18]. When the dynamic vibration absorber lacks tuning, vibrations become more pronounced at specific natural frequencies: 23 Hz in the z-axis and 27 Hz in the x and y axes. Employing a fixed tuning at 23 Hz amplifies vibrations at higher frequencies, potentially surpassing the original vibration amplitude. Likewise, a fixed tuning at 27 Hz results in elevated vibration values both below and above that frequency. In contrast, the self-tuning approach consistently achieves the lowest vibration levels, demonstrating

superior performance compared to conventional fixed damping systems, particularly for structures with multiple modes.

Jeong's research concentrates on the attenuation of vibrations in systems characterized by varying excitation frequencies [19]. The focus involves the creation and experimentation of a tunable dynamic vibration absorber employing MRE. The adaptive tuned dynamic vibration absorber design integrates stiffness and mass as critical components. For the stiffness element, the specimen thickness is determined by assessing the rate of change of the MRE's shear modulus concerning its thickness. The mass element is optimized through sensitivity analysis and genetic algorithms, utilizing formulated equations for its magnetic field and mass. The implementation of an electric current to the MRE allows for the measurement of its stiffness, facilitating the adjustment of the designed MRE-based adaptive tuned dynamic vibration absorber. The study concludes by evaluating the vibration reduction performance of the MRE-based absorber, assessing its suitability under variable-frequency excitation conditions.

Rubio, Loya, Miguélez, and Fernández-Sáez tried to optimize parameters for a passive dynamic vibration absorber connected to a boring bar. [20]. The boring bar was conceptualized as an Euler-Bernoulli cantilever beam, and a comprehensive analysis of the system's stability was conducted, taking into account the characteristics of both the bar and the absorber. The researchers derived optimal parameters for the absorber by employing a classical method for solving optimization problems without constraints. The objective was to maximize the smallest values indicated on the stability lobe diagram.. Empirically derived expressions detailing the damping ratio frequency of the dynamic vibration absorber were utilized to determine its stiffness and damping. These expressions prove particularly valuable when dealing with practical operations where the damping ratio of the boring bar exhibits non-zero value. The computational results demonstrated a distinct enhancement in stability performance compared to previously utilized methodologies.

Aliakbari, Moraru, Veron, and Groll examined the Steadyline anti-vibration toolholder to assess its effectiveness in dealing with chatter issues [21]. This technology incorporates a significant mass in the boring bar, supported by adjustable rubber O-rings. Using experimental modal analysis, they studied deflection shapes at natural frequencies and anti-resonance within the relevant frequency range, providing insights into the dynamic characteristics of the bar. The findings indicated that Steadyline demonstrates amplitude-dependent characteristics attributed to the intrinsic properties of rubber-like materials containing carbon black fillers. While impact hammer tests helped determine optimal configurations, they were considered less reliable for nonlinear amplitude-dependent systems. Inconsistencies in dynamic behavior were observed due to variations in geometric tolerances and uncertainties in material properties in the rubber O-rings, even for identical bars.

Hua, Wong, and Cheng introduced a beam-based dynamic vibration absorber and compared it with the traditional discrete mass-spring-damper system [22]. The proposed beam absorber demonstrated superior vibration reduction under the same mass ratio compared to the traditional dynamic vibration absorber. In contrast to the conventional spring-mass-damper system, which is limited in optimal performance by the mass ratio, the beam absorber can surpass its counterpart while adhering to equivalent mass ratio constraints, given the appropriate material and geometric parameters.

2.2 Fatigue Life Estimation Methods

In this section, fatigue life estimation procedure of a metal vibration isolator has been defined. In order to evaluate the fatigue life of a vibration isolator, power spectrum responses for displacement, stresses or strains can be needed. One of the cumulative fatigue damage theories has to be used. These are categorized like stress-based, strain-based and energy based approaches. Fatigue crack propagation method will not be used because of the difficulty of determining the time when crack initiates and starts to grow. Steinberg, Narrow-Band and Wirching methods can be used in

frequency domain solution of damage calculation in ANSYS. In this thesis work, stress based approach is used to estimate the metal vibration isolator life.

Eldoğan and Cigeroglu have worked on the vibration fatigue analysis of a cantilever beam and they compared the results of time domain and frequency domain methods [23]. The analysis shows that the fatigue life result obtained from Dirlik method is considerably similar to that of Rainflow counting method. Moreover, the significant conclusion of the study is about the effect of damping ratio on the fatigue life estimation. It is reported that the accuracy of the damping ratio has significant effect in terms of accurate determination of fatigue life. Therefore, while performing the calculation of the damping ratio, it is imperative to attain values that closely align with actual conditions. Otherwise, unforeseen failures could potentially manifest during operational phases.

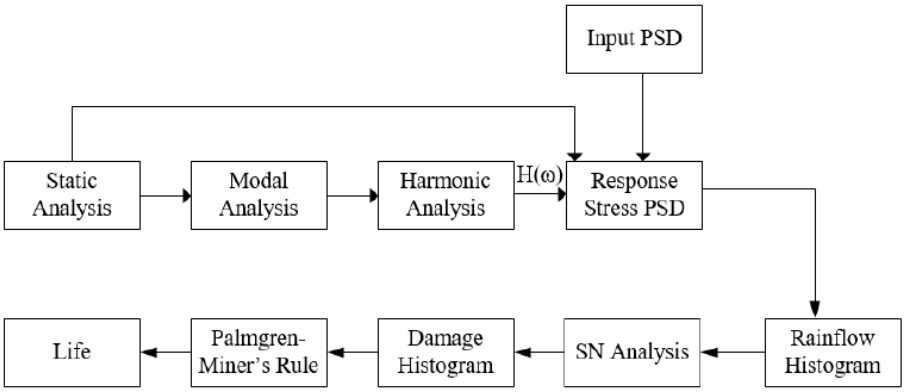

Figure 2.1 Fatigue Life Estimation Procedure Diagram [24]

During the finite element analysis calculation, Figure 2.1 is taken as a reference procedure chart. Figure shows that life estimation starts with some static, modal and harmonic analyses and then, input is imported to the process to obtain stress PSD output. After that one of the damage accumulation method can be used to predict life of a designed metal vibration isolator.

Miner's Rule [25] is employed to assess damage resulting from cyclic or time-dependent loading. Serving as a linear model for damage accumulation, Miner's Rule

utilizes a load-time history and an S-N curve as input to compute damage. The mathematical expression for Miner's Rule is given by:

$$D = \sum_i d_i = \sum_i \frac{n_i}{N_i} \tag{2.1}$$

Here, D represents cumulative damage, d_i denotes fatigue damage in each cycle, n_i signifies the expected number of cycles at a given stress level σ_i, and N_i indicates the number of cycles until failure at the same stress level as determined from the S-N fatigue life curve.

When the cumulative damageattains a value of "1," it signifies the occurrence of failure. The definition of failure in the context of a physical component exhibits variability. This could imply the initiation of a crack on the surface of the component. Alternatively, it may denote the complete traversal of a crack through the entirety of the component, leading to its separation.

CHAPTER 3

CONCEPT DEVELOPMENT

This chapter comprises three sections. Initially, it provides insight into the prior study, which serves as the foundation for this thesis. Subsequently, it observes the impact of applying the Tuned Vibration Absorber (TVA) on the test configuration of this study. Finally, it addresses the determination of the target mode for enhancing damping through the application of TVA.

3.1 About Previous Study

In this section, the vibration isolation system previously designed by Karaman for spacecraft launch vehicles is presented along with potential areas for improvement [26].

It revolves around the design and validation of innovative vibration isolation systems for space launch vehicles, with a focus on reducing the transmission of high-level vibration loads from the launch vehicle to the payload. During launch, payloads, including satellites and spacecraft, are subjected to substantial vibrational forces that can potentially harm the payload. To address this challenge, vibration isolation systems are considered at the interface between the payload and launch vehicle as shown in Figıure 3.1.

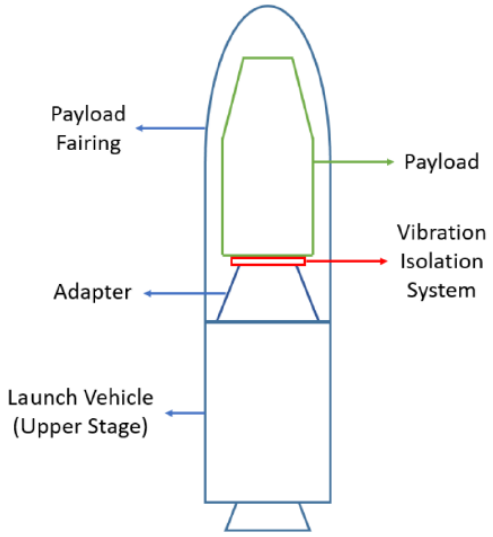

Figure 3.1 Schematic of Vibration Isolation System for Space Launch Vehicle [26]

In that study, the Dnepr launch vehicle and Sentinel-2 satellite are selected as a case study. The research begins by establishing system-level technical requirements for the vibration isolation system. Key properties of the vibration isolators, including stiffness, loss factor, and quantity, are determined to align with these technical requirements. This determination is accomplished through mathematical modeling, encompassing random response and harmonic response analyses.

The study progresses to conceptualize six distinct vibration isolator concepts, utilizing methodologies such as topology optimization and compliant mechanisms. Subsequently, detailed designs for three different vibration isolator alternatives are conducted to achieve the necessary stiffness and loss factor values. The designed vibration isolators are shown in Figure 3.2, Figure 3.3 and Figure 3.4. Finite element analyses are employed to accurately evaluate the stiffness and loss factor of these isolators.

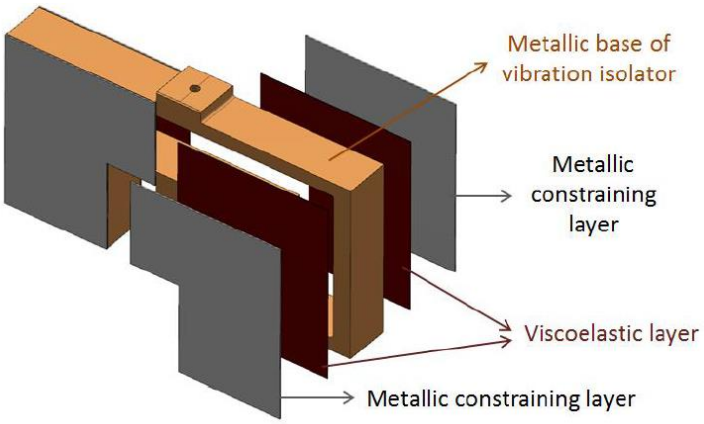

Figure 3.2 Vibration Isolator Damping Concept, S1 [26]

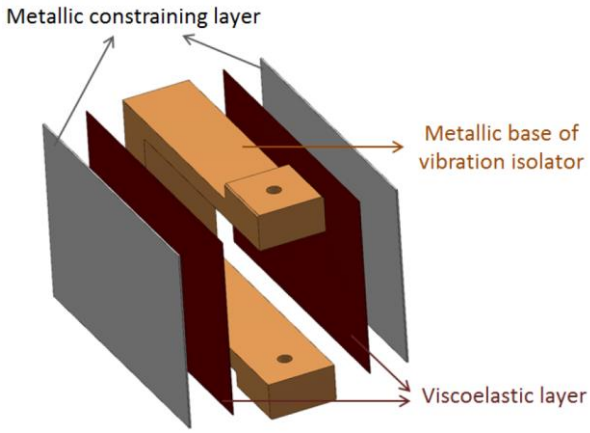

Figure 3.3 Vibration Isolator Damping Concept, T1 [26]

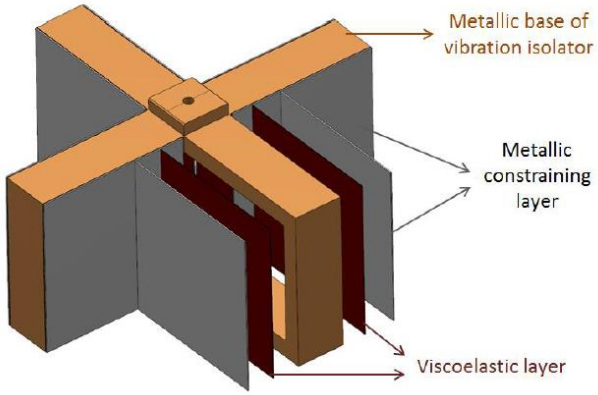

Figure 3.4 Vibration Isolator Damping Concept, T2 [26]

Ultimately, the designed vibration isolation systems, which is shown in Figure 3.5 for T1, undergo comprehensive validation through finite element analyses and vibration tests in a controlled laboratory environment. Test setup of T1 is shown in Figure 3.6. Scaling down to one-twentieth of its original size was performed to simulate a weight of 1.2 tons on the isolation system composed of 60 isolators. Similar experimental testing was conducted on other concepts.

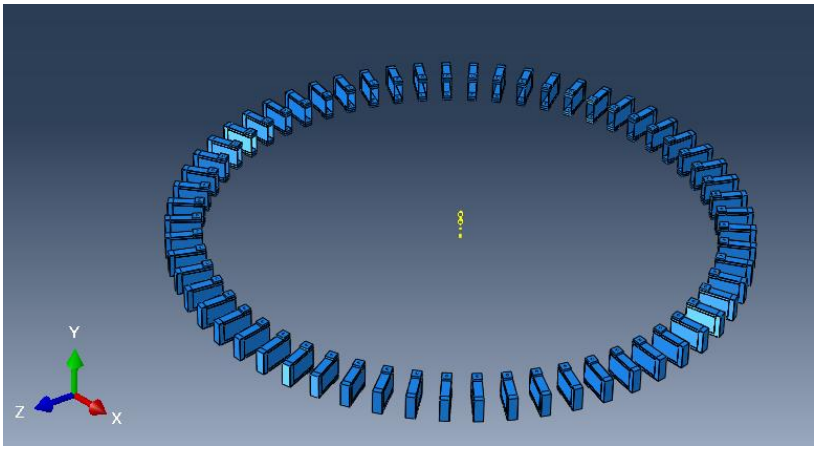

Figure 3.5 Vibration Isolation System Consisting of 60 Isolators

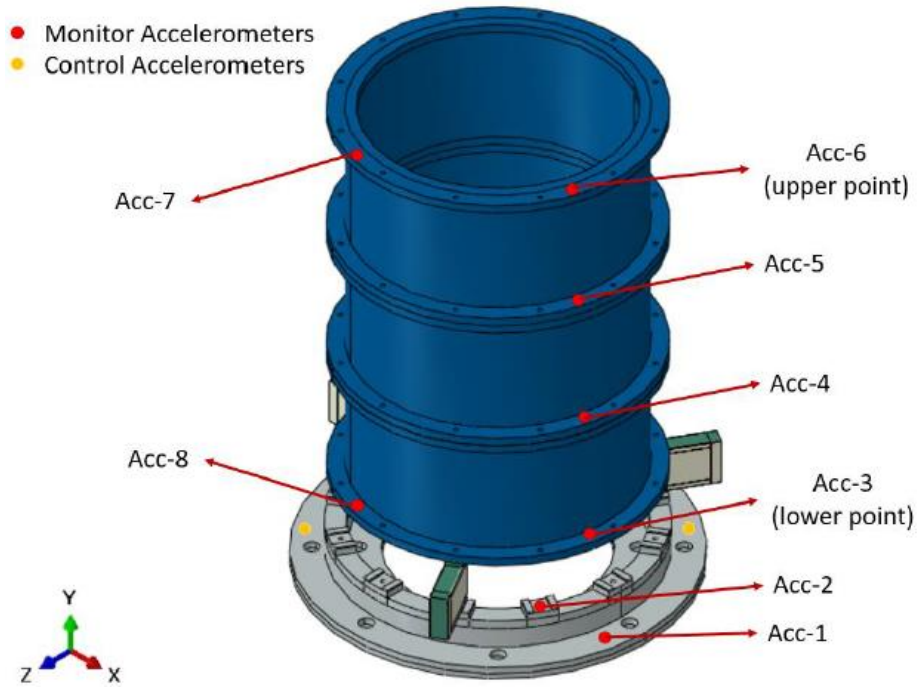

Figure 3.6 Test Setup of T1 [26]

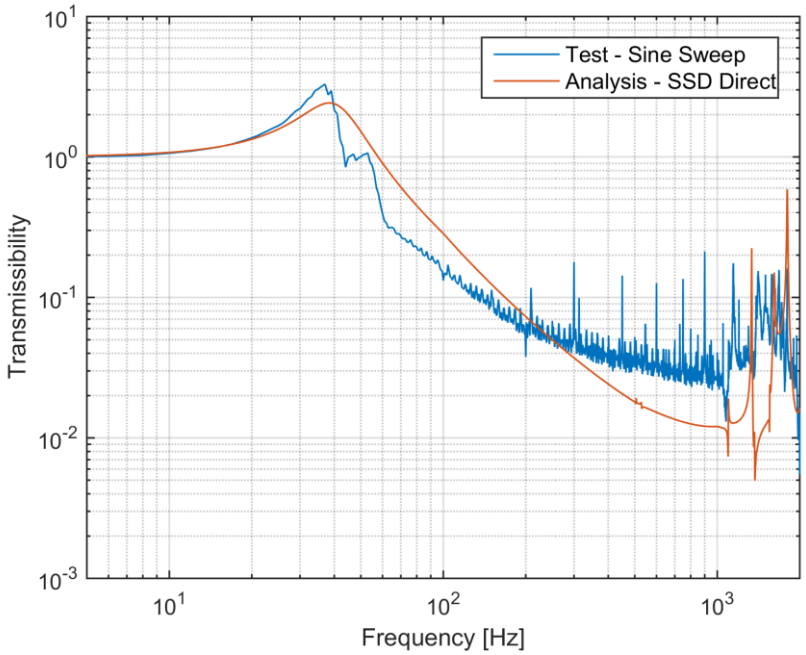

Figure 3.7 The comparison of axial transmissibility curves obtained from sine sweep test and finite element analysis for upper point [26]

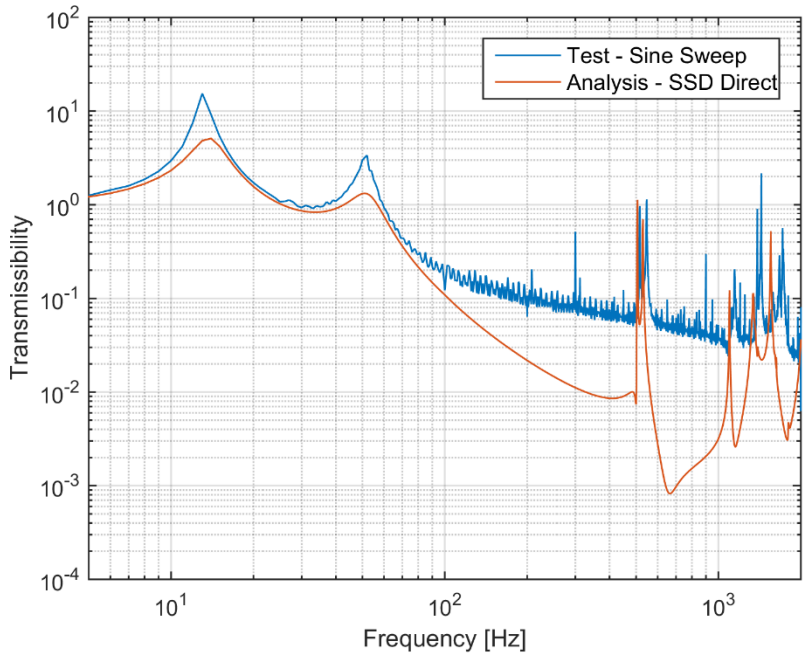

Figure 3.8 The comparison of lateral transmissibility curves obtained from sine sweep test and finite element analysis for upper point [26]

After the tests, when examining the transmissibility plots in the axial and lateral directions, peaks are observed at high frequencies, which it is attributed to internal resonance of the isolator. Moreover, the observation was made that the T1 component had fractured. Recognizing these as a research topic requiring further investigation, this thesis hypothesizes that the fracture may be attributed to low internal damping at high-frequency resonance points. Therefore, efforts are made in this thesis to address and mitigate this issue. Additionally, fatigue life estimation is conducted to demonstrate that the applied solution does not have a detrimental effect on the system's lifespan, as this is one of the main focuses of this thesis.

3.2 TVA Applicability Demonstration

A tuned vibration absorber is a special device designed to control unwanted vibrations in machines and structures. It works by using a carefully adjusted mass and spring system to absorb vibrations at specific frequencies. The device is connected to the structure, and the mass is tuned to vibrate at the same frequency as the unwanted vibrations. By doing this, the absorber can effectively cancel out the undesired vibrations, making the system more stable. In this section, an investigation was conducted to assess the potential structural improvements resulting from the envisaged application of the TVA on the triple configuration previously subjected to testing. The primary objective of this section is to scrutinize the applicability of implementing the TVA, with particular attention to its effects on the fractured T1 component observed in the earlier test structure. Firstly, two cases are investigated, where the payload behaves flexibly and rigidly. the aim of the first case is to identify the peak points in the transmissibility plots in Figure 3.7 and Figure 3.8. Moreover, the aim of the second case is to find out the resonance frequencies of isolators. Subsequently, the flexible structure of the triple test configuration is used as a reference during the TVA study. Studies are conducted for the TVA application in only the axial direction, only the lateral direction, and subsequently, in both

directions together. TVAs are added to the all of these 3 isolators in a same manner, which representations are shown in Figure 3.9 and Figure 3.10.

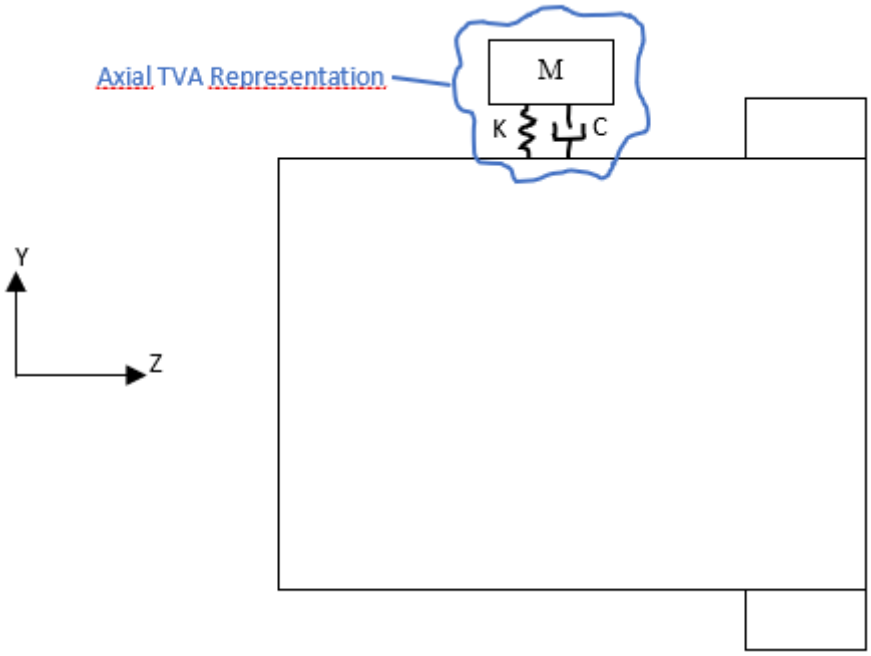

Figure 3.9 Axial TVA representation

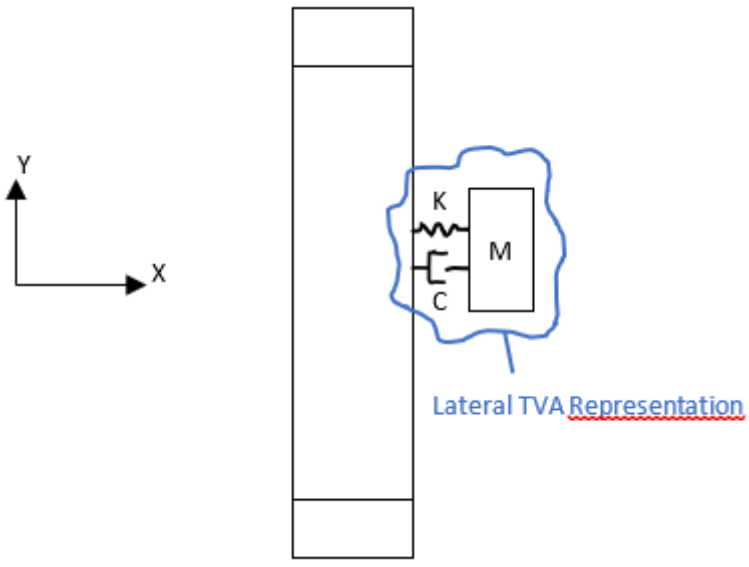

Figure 3.10 Lateral TVA Representation

As a first case, the mode shapes and resonance frequencies of the triple test structure have been examined by reducing the density of the VEM layer to avoid unwanted internal resonances of VEM layer. The constrained layer damping solution employed in this research is 3M Damping Foil 2552, which incorporates a viscoelastic polymer, ISD 112, in tandem with an aluminum foil backing. The viscoelastic material possesses a thickness of 0.127 mm, while the constraining layer has a thickness of 0.254 mm. The supplier has furnished the shear modulus and loss factor nomograph for ISD 112, which is shown in Figure 3.11.

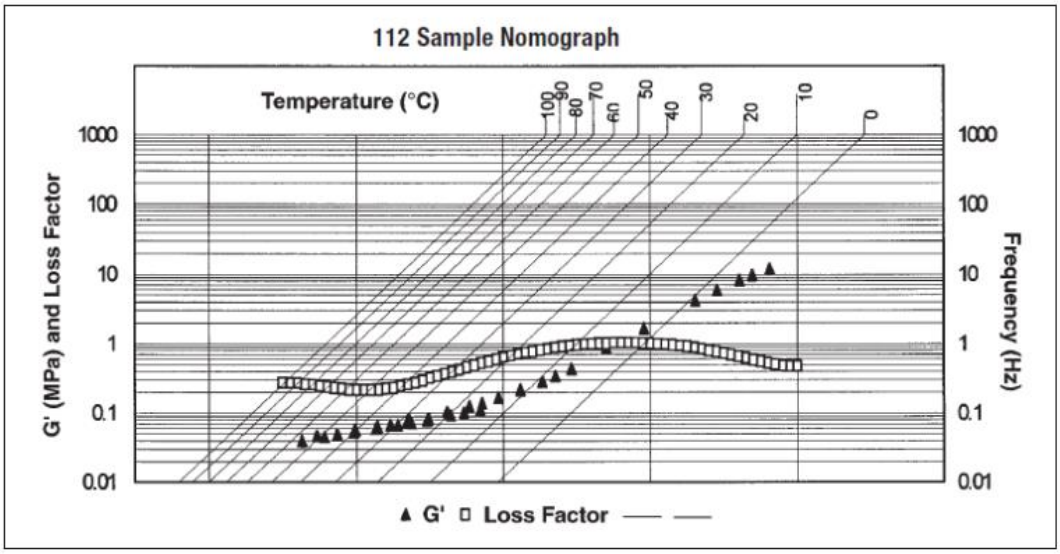

Figure 3.11 Nomograph of Viscoelastic Damping Polymer 112 Series [27]

The nomograph in Figure 3.11 can be interpreted as follows. The determination of loss factor and storage modulus values for the 3M viscoelastic damping polymer 112 involves selecting the desired application frequency and extending a horizontal line from that frequency until it intersects the desired application temperature isotherm. Subsequently, a vertical line is extended from the initial point of intersection between the desired frequency and temperature isotherm, intersecting the curves representing loss factor and storage modulus. The corresponding values of loss factor and storage modulus are then ascertained on the left-hand scale by drawing a horizontal line from the points where the loss factor and storage modulus performance curves intersect for the second time. While bonding VEM layer with flexure element, tie contact is

defined with the partitioned surfaces. The base holes of the base fixture have been fixed as BC. The obtained resonance frequencies of the transmissibility plots are shown in Table 3.1.

Table 3.1 Resonance Frequencies of Triple Test Structure

	0-100 Hz Resonances	100-2000 Hz Resonances				
Axial Direction	38	1335	1610	1800	-	-
Lateral Direction	14 - 51	506	529	1097.5	1338	1554

As a second case, an investigation has been conducted on the mode shapes in the triple test structure when the Young's Modulus of the payload has been increased to induce rigid behavior to the payload. The base holes of the base fixture have been fixed as BC. The internal resonances and mode shapes of the isolator, obtained by considering the payload as rigid, are shown in Figure 3.12 and Figure 3.13.

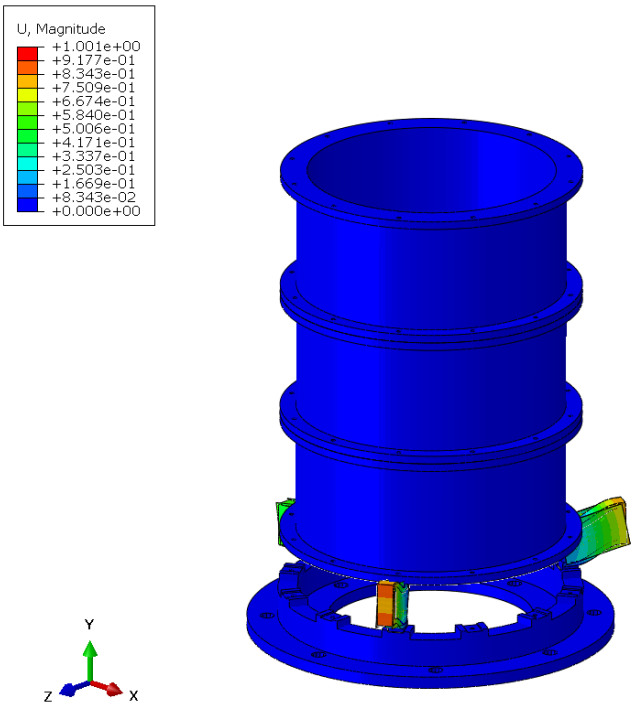

Figure 3.12 Internal Resonance of Isolator, 1338 Hz

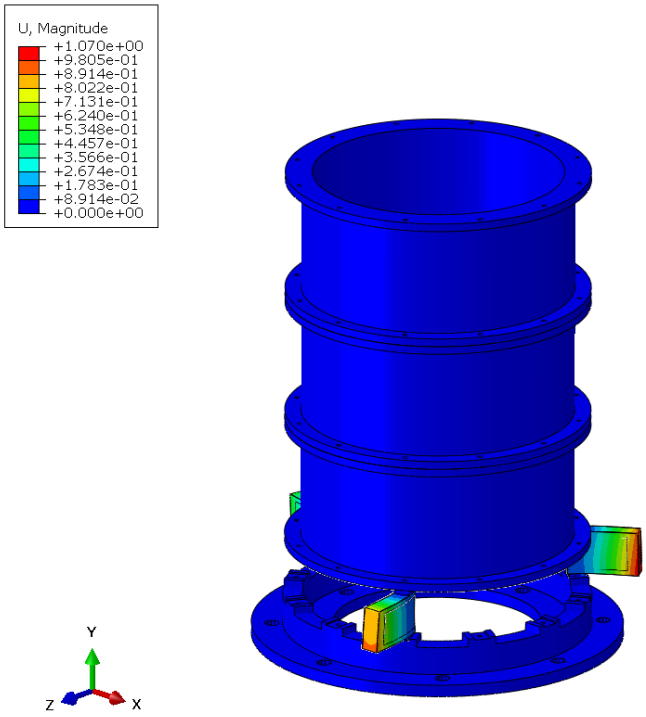

Figure 3.13 Internal Resonance of Isolator, 1380 Hz

3.2.1 Axial TVA Implementation

There are three peaks identified at high frequencies in the axial direction. These peaks are shown in Figure 3.14 and Table 3.2. Note that transmissibility data is taken at the upper point shown in Figure 3.6 to be consistent with previously obtained results.

Table 3.2 Resonance Frequencies of Triple Test Structure in Axial Direction

	0-100 Hz Resonances	100-2000 Hz Resonances				
Axial Direction	38	1335	1610	1800	-	-

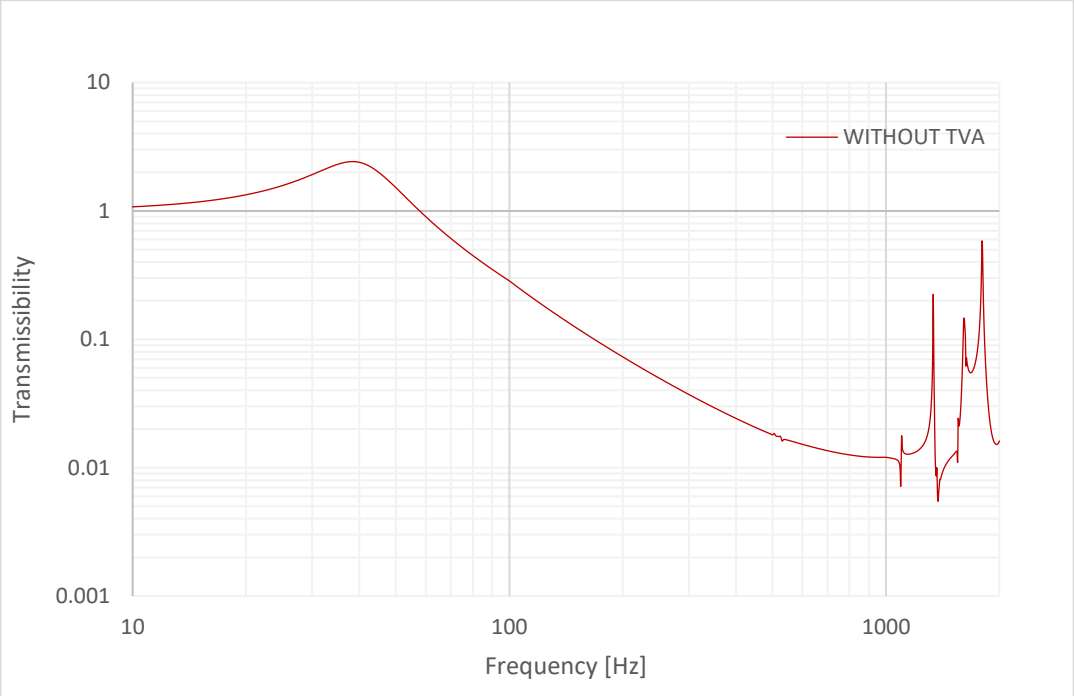

Figure 3.14 Transmissibility Plot in Axial Direction Without TVA Implementation

Initially, TVAs are tuned to 1800 Hz. These TVAs are placed outward on the upper surface of the isolators as shown in Figure 3.15.

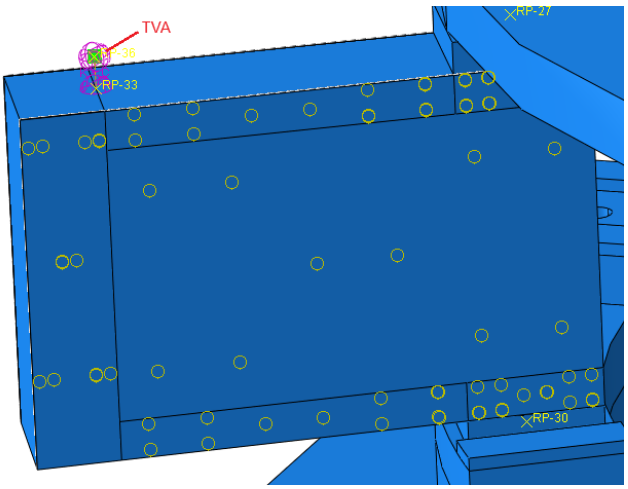

Figure 3.15 Location of TVA Tuned at 1800 Hz

TVA implementations are carried out using the ABAQUS software. In this software, TVA is defined as a mass-spring-dashpot system. Information such as mass, spring stiffness, and dashpot coefficient is required for this definition. The procedure followed is as shown below while defining TVA tuned at a specific frequency.

Firstly, the frequency which TVA is tuned is chosen.

$$\omega_d = \omega_n\sqrt{1-\zeta^2} \tag{3.1}$$

where ω_d is the tuning frequency of TVA, ω_n is the natural frequency and ζ is the damping ratio. Then, required damping ratio is decided, and natural frequency required for this procedure is obtained from Equation (3.1).

$$\omega_n = \sqrt{\frac{k}{m}} \tag{3.2}$$

where k is the spring stiffness and m is the mass. After obtaining natural frequency, stiffness is calculated for a specific mass from Equation (3.2).

$$c = 2 \cdot \zeta \cdot \sqrt{k \cdot m} \tag{3.3}$$

Finally, c, which is dashpot coefficient, is found by using Equation (3.3)

The parameter information for TVAs tuned to 1800 Hz for different masses are shown in Table 3.3. ABAQUS uses Newton-Tonne-mm unit system. Therefore, the units of the parameters in Table 3.3 have been adjusted accordingly to this system.

Table 3.3 TVA Parameters for 1800 Hz

	Mass [Tonne]	**Spring Stiffness [N/mm]**	**Dashpot Coefficient [N.s/mm]**	**Damping Ratio**
P1	0.000005	852.75	0.065297	0.5
P2	0.000010	1705.5	0.130594	0.5
P3	0.000020	3411	0.261189	0.5
P4	0.000040	6822	0.522379	0.5

During the parametric study, the mass is added as a point mass and constrained with spring-dashpot. As seen in Figure 3.16 and Figure 3.17, point mass is coupled with spring-dashpot, and only allowed to move in the direction perpendicular to the constrained surface. Reference points are added to the point mass location and the spring location on the surface of the isolator. Then, these reference points are linked to each other and the surface through a "coupling" constraint type in ABAQUS.

Unit amplitude sin wave is subsequently exerted to fixture holes over the relevant frequency range. It has to be noted that other directions are fixed apart from sin wave is applied as BC. ABAQUS analysis involves the utilization of the "Steady-state dynamics, Direct" step, which is appropriate for specifying frequency-dependent viscoelastic properties. Therefore, upcoming results are obtained by using "Steady-state dynamics, Direct" step,

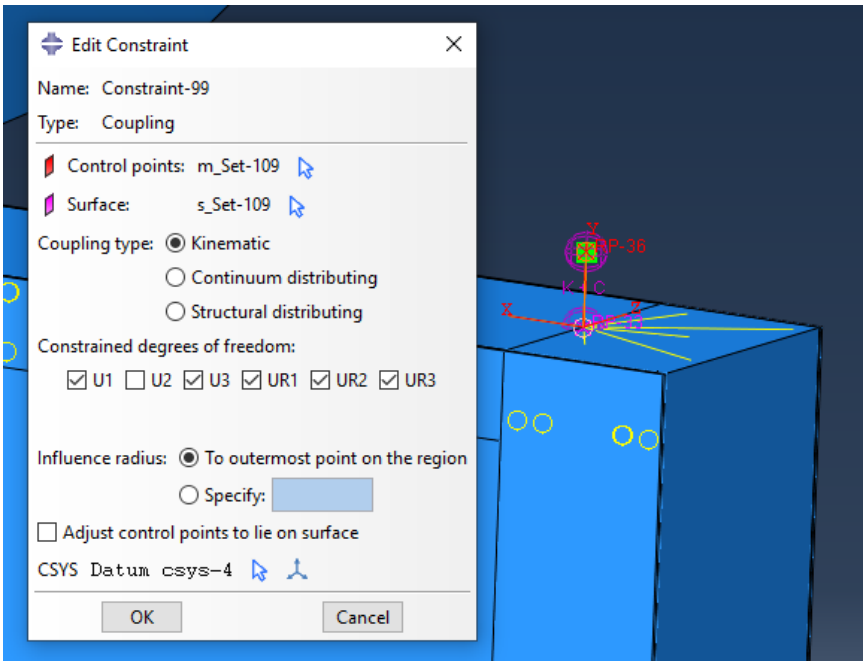

Figure 3.16 Kinematic Coupling of Mass-Spring-Dashpot System

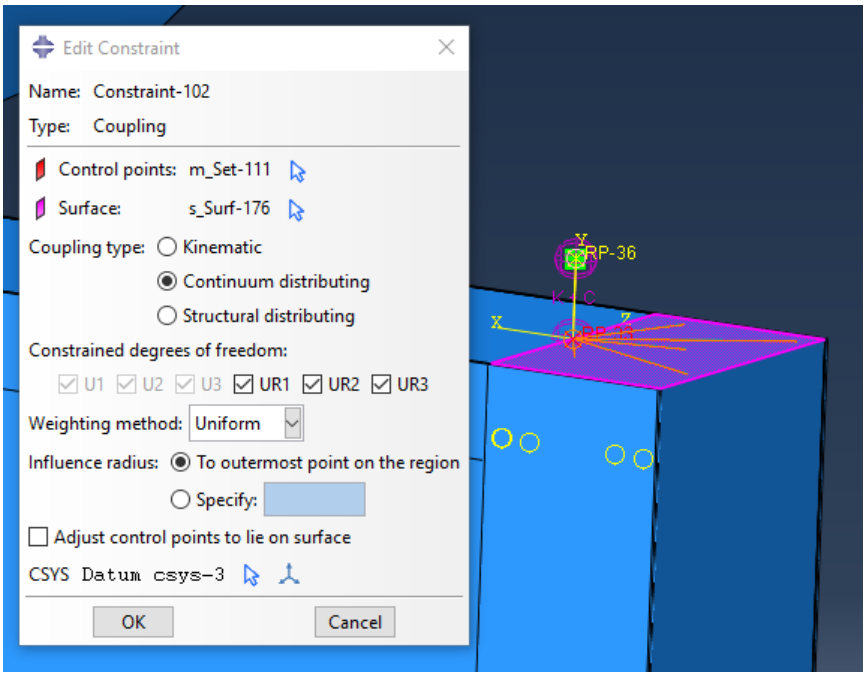

Figure 3.17 Continuum Distributing Coupling of Mass-Spring-Dashpot System

Table 3.4 TVA Parametric Results for 1800 Hz in Axial Direction

	Without TVA	**P1**	**P2**	**P3**	**P4**
Transmissibility Peak Value at 1800 Hz	0.5857	0.4595	0.4289	0.4736	0.6030

Comparative results obtained for the three peak values for the better option, P2, are provided in Table 3.5.

Table 3.5 Transmissibility Comparison of Without TVA and P2 in Axial Direction

	Axial Transmissiblity at Resonance Frequency		
	Peak at 1335 Hz	**Peak at 1610 Hz**	**Peak at 1800 Hz**
Without TVA	0.224	0.146	0.5857
P2	0.081	0.1616	0.429

According to the results, the addition of TVAs at 1800 Hz demonstrates an improvement in the peak values both at 1335 Hz and 1800 Hz. Transmissibility improvement at 1335 Hz is attributed to the vertical mode shape occuring at the internal resonance of the isolators. Consequently, a secondary TVA application is planned, wherein TVAs are tuned to 1335 Hz and strategically placed at the center of the upper surface. A similar parametric study is conducted to further investigate the system's response. In this parametric study, P2 and TVAs at 1335 Hz are used together as shown in Figure 3.18.

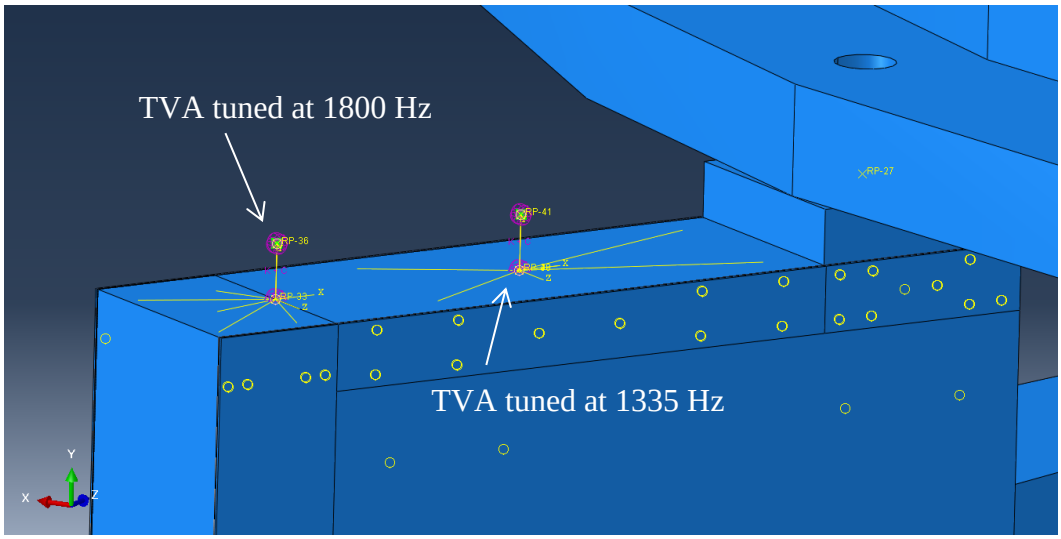

Figure 3.18 Location of TVAs Tuned at 1335 and 1800 Hz

The parameter information for TVAs tuned to 1335 Hz for different masses are shown in Table 3.6. Damping ratio is chosen by referencing the need of high damping at these frequencies. It is believed that low damping capability of isolators at higher resonance frequencies is causing these peaks.

Table 3.6 TVA Parameters for 1335 Hz

	Mass [Tonne]	**Spring Stiffness [N/mm]**	**Dashpot Coefficient [N.s/mm]**	**Damping Ratio**
P5	0.000010	1099.7	0.125839	0.6
P6	0.000020	2199.4	0.251679	0.6
P7	0.000030	3299.1	0.377519	0.6
P8	0.000045	4948.65	0.566279	0.6
P9	0.000060	6598.2	0.755039	0.6

Table 3.7 Double TVA Parametric Results in Axial Direction

	Without TVA	**P2+P5**	**P2+P6**	**P2+P7**	**P2+P8**	**P2+P9**
Transmissibility Peak Value at 1335 Hz	0.224	0.0651	0.0644	0.0536	0.0531	0.0531
Transmissibility Peak Value at 1610 Hz	0.146	0.1529	0.1539	0.1544	0.1593	0.1819
Transmissibility Peak Value at 1800 Hz	0.5857	0.4368	0.4023	0.3776	0.3529	0.3378

When examining Table 3.7, it is observed that combined use of P2 and P8 has good capability except for the peak occuring at 1600 Hz. In other words, adding TVAs tuned to 1800 Hz with a mass of 10 grams on the left and TVAs tuned to 1335 Hz with a mass of 45 grams on the right of the upper surface of the isolators result in a decrement at the peaks apart from that one occuring at 1600 Hz. The incorporation of P8 demonstrates improvement across all peaks compared to P2. Consequently, an

exclusive analysis is conducted to obtain the results for the single usage of P8. The comparison about without using TVA, using only TVAs tuned at 1800 Hz, using TVAs tuned at 1335 Hz and 1800 Hz together and using only TVAs tuned at 1335 Hz is made in Table 3.8.

Table 3.8 Transmissibility Comparison of Without TVA, P2, P2+P8 and P8 in Axial Direction

	Axial Transmissiblity at Resonance Frequency		
	Peak at 1335 Hz	**Peak at 1610 Hz**	**Peak at 1800 Hz**
Without TVA	0.224	0.146	0.5857
P2	0.081	0.1616	0.429
P2+P8	0.0531	0.1593	0.3529
P8	0.0529	0.1299	0.2875

Upon examining the comparative results in Table 3.8, it is evident that the optimal choice is the single use of a TVA tuned to 1335 Hz. The reason for obtaining such a result lies in the mode shape of the isolators at that frequency, which involves vertical up-and-down movement. The comparison plot of the tranmissibilities are plotted in Figure 3.19.

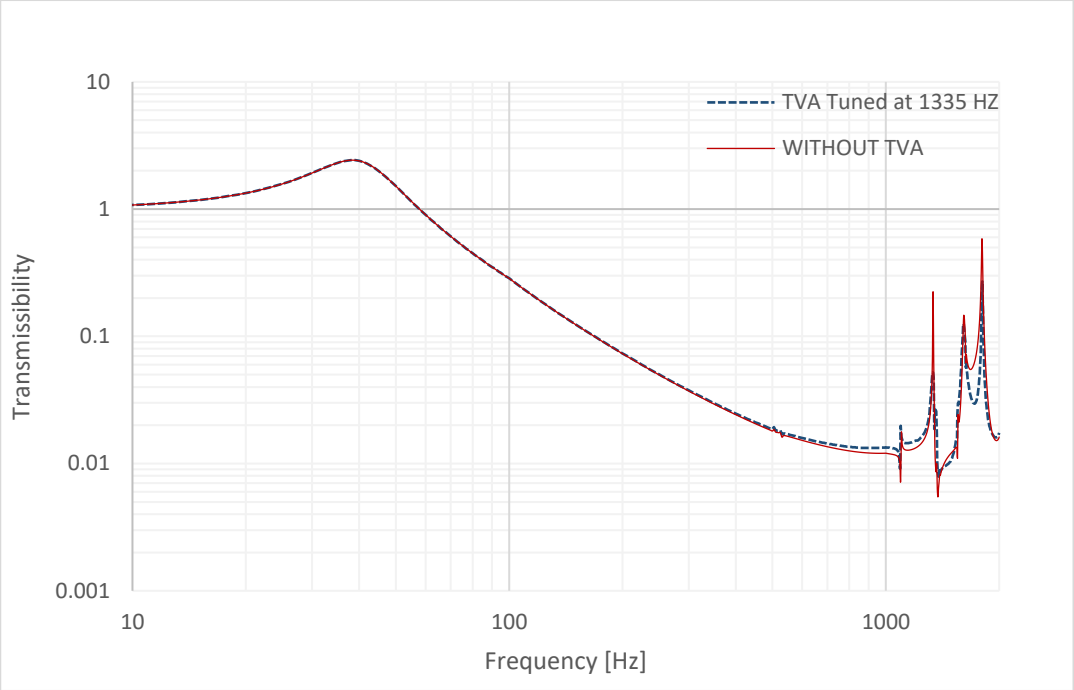

Figure 3.19 Transmissibility Comparison Plot in Axial Direction for TVA Applied Only Upper Surface at 1335 Hz

3.2.2 Lateral TVA Implementation

There are five peaks identified at high frequencies in the lateral direction. These peaks are shown in Figure 3.20 ant Table 3.9. Note that transmissibility data is taken at the upper point shown in Figure 3.6 to be consistent with previously obtained results.

Table 3.9 Resonance Frequencies of Triple Test Structure in Lateral Direction

	0-100 Hz Resonances	100-2000 Hz Resonances				
Lateral Direction	14 - 51	506	529	1097.5	1338	1554

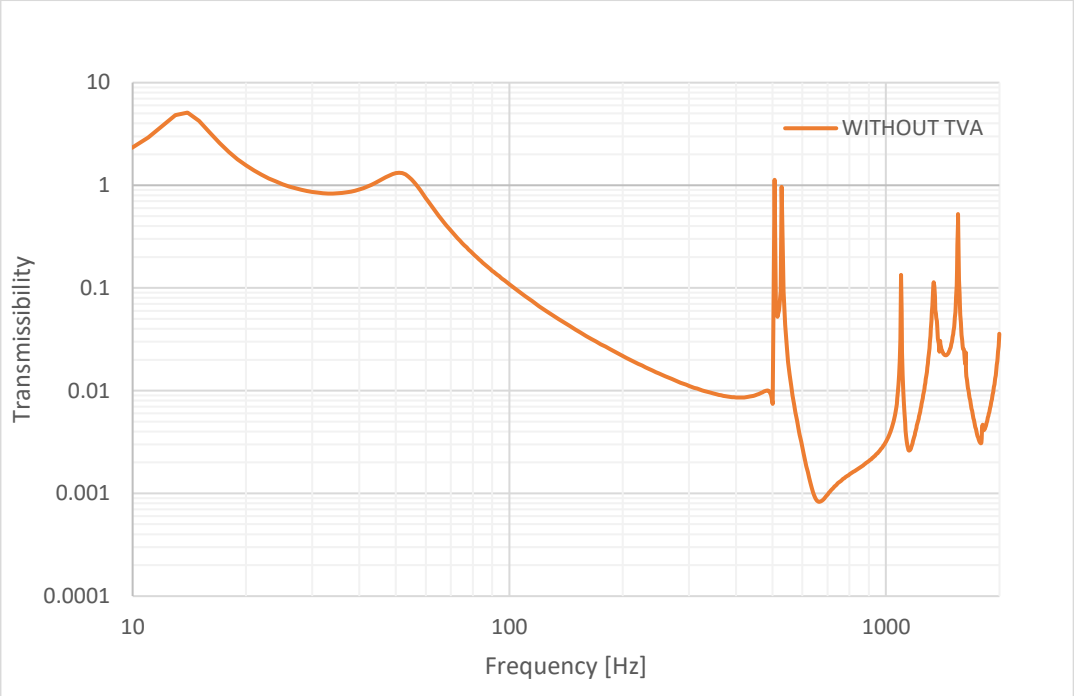

Figure 3.20 Transmissibility Plot in Lateral Direction Without TVA Implementation

TVAs tuned at 1338 Hz are located on the outer middle part of the lateral surface of the isolators as shown in Figure 3.21. Moreover, the parameter information for TVAs tuned to 1338 Hz are shown in Table 3.10.

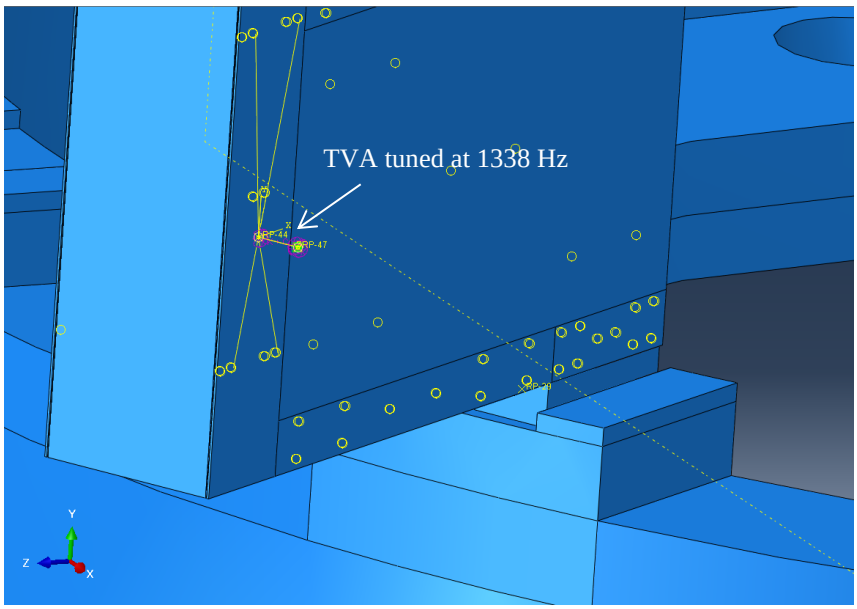

Figure 3.21 Location of TVA Tuned at 1338 Hz

Table 3.10 TVA Parameters for 1338 Hz

	Mass [Tonne]	**Spring Stiffness [N/mm]**	**Dashpot Coefficient [N.s/mm]**	**Damping Ratio**
P10	0.000010	1104.31	0.126103	0.6
P11	0.000015	1656.465	0.189155	0.6
P12	0.000030	3312.93	0.378310	0.6

Table 3.11 Transmissibility Comparison of Without TVA, P10, P11 and P12 in Lateral Direction

	Lateral Transmissiblity at Resonance Frequency				
	Peak at 506 Hz	**Peak at 529 Hz**	**Peak at 1097.5 Hz**	**Peak at 1338 Hz**	**Peak at 1554 Hz**
Without TVA	1.126	0.965	0.134	0.114	0.523
P10	1.266	0.967	0.037	0.022	0.429
P11	1.155	0.933	0.267	0.025	0.393
P12	0.553	0.689	0.497	0.036	0.326

Upon examining the comparative results, it is obvious that the optimal choice is P10. Moreover, it is observed that increase in mass results in decrease for the peak at 1554 Hz while increasing transmissibility values for the peak occuring at 1097.5 Hz and 1338 Hz.

3.2.3 Both Axial and Lateral TVA Implementation

In this section, it is presented the results of the concurrent utilization of the obtained axial and lateral TVAs. The influence of TVAs on peaks in the other axis, considering both axial and lateral directions, is also examined, and an optimization process is undertaken to obtain best results. The optimal option is attained when improvement is observed in the transmissibility values at each frequency.

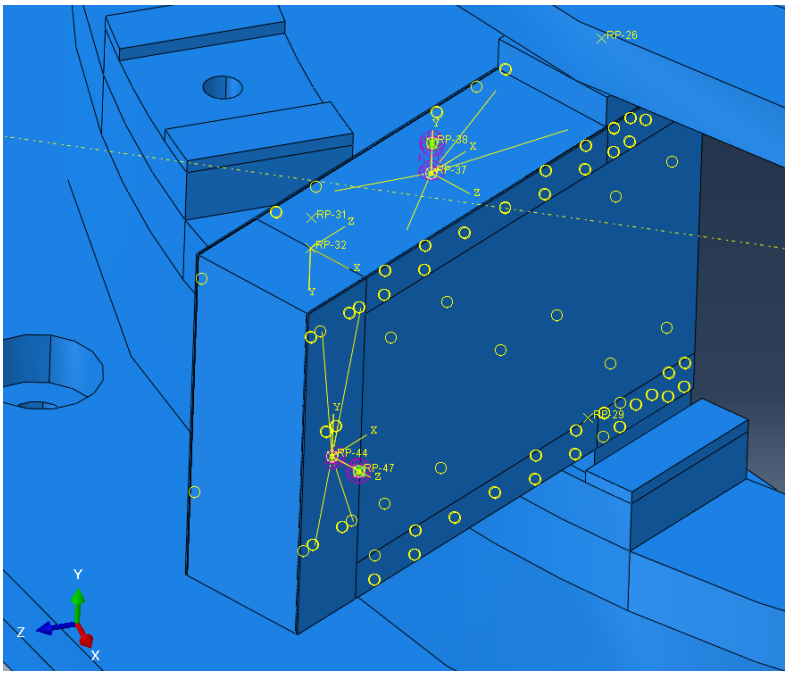

Figure 3.22 Location of TVA Tuned at 1335 Hz and 1338 Hz

In the forthcoming tables of the optimization study, cells highlighted in red color signify a degradation in the transmissibility value at the respective frequency, yellow color indicates no change, and green color represents an improvement. The axial and lateral results of the combined use of P8 and P10, which their locations are shown in Figure 3.22, are presented in Tables 3.12 and 3.13 utilizing that color scheme.

Table 3.12 Transmissibility Comparison of Without TVA and P8+P10 in Axial Direction

	Axial Transmissiblity at Resonance Frequency		
	Peak at 1335 Hz	**Peak at 1610 Hz**	**Peak at 1800 Hz**
Without TVA	0.224	0.146	0.5857
P8+P10	0.0526	0.123	0.2857

Table 3.13 Transmissibility Comparison of Without TVA and P8+P10 in Lateral Direction

	Lateral Transmissiblity at Resonance Frequency				
	Peak at 506 Hz	**Peak at 529 Hz**	**Peak at 1097.5 Hz**	**Peak at 1338 Hz**	**Peak at 1554 Hz**
Without TVA	1.126	0.965	0.134	0.114	0.523
P8+P10	0.207	0.632	0.338	0.0221	0.532

In an effort to enhance the outcome indicated red color in Table 3.13, a third TVA tuned to 1097.5 Hz is added to the center of the upper surface on the side where the lateral TVA is located shown in Figure 3.23. Detailed information regarding the parameters to be utilized can be found in Table 3.14, while the lateral transmissibility values obtained from triple TVA usage for these parameters are presented in Table 3.15.

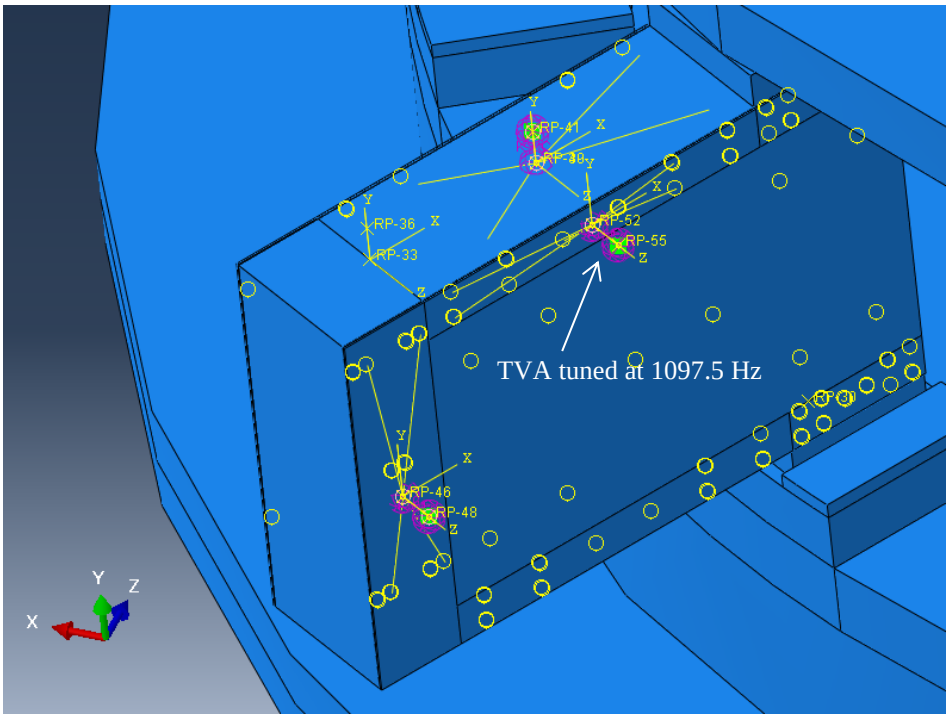

Figure 3.23 Location of TVA Tuned at 1335 Hz, 1338 Hz and 1097.5 Hz

Table 3.14 TVA Parameters for 1097.5 Hz

	Mass [Tonne]	**Spring Stiffness [N/mm]**	**Dashpot Coefficient [N.s/mm]**	**Damping Ratio**
P13	0.000005	371.5	0.051718	0.6
P14	0.000010	743	0.103436	0.6
P15	0.000015	1114.5	0.155155	0.6
P16	0.000020	1486	0.206873	0.6
P17	0.000025	1857.5	0.258592	0.6
P18	0.000030	2229	0.310311	0.6

Table 3.15 Triple TVA Parametric Results in Lateral Direction

	Lateral Transmissiblity at Resonance Frequency				
	Peak at 506 Hz	**Peak at 529 Hz**	**Peak at 1097.5 Hz**	**Peak at 1338 Hz**	**Peak at 1554 Hz**
Without TVA	1.126	0.965	0.134	0.114	0.523
P8+P10+P13	0.176	0.670	0.267	0.0222	0.479
P8+P10+P14	0.1508	0.71	0.257	0.0216	0.426
P8+P10+P15	0.131	0.748	0.247	0.0198	0.39
P8+P10+P16	0.115	0.779	0.244	0.0169	0.386
P8+P10+P18	0.1	0.782	0.207	0.0134	0.391

Upon examination of the results, it becomes evident that the influence of incorporating the third TVA at 1097.5 Hz becomes more pronounced with an increasing mass. However, it has not completely approached the transmissibility value of the original structure without TVA. Furthermore, an increase in the mass of the third TVA results in a simultaneous deterioration observed at the second peak. Consequently, a configuration with a mass of 20 grams in the triple TVAs setup is selected. The first TVA added to the lateral surface is omitted, leaving only the axial

TVA and TVA tuned at 1097.5 Hz. This adjustment is implemented to ascertain whether the observed increase at the third peak could be attributed to TVA tuned at 1338 Hz. The depicted structure is illustrated in Figure 3.24, and the comparative results are detailed in Table 3.16.

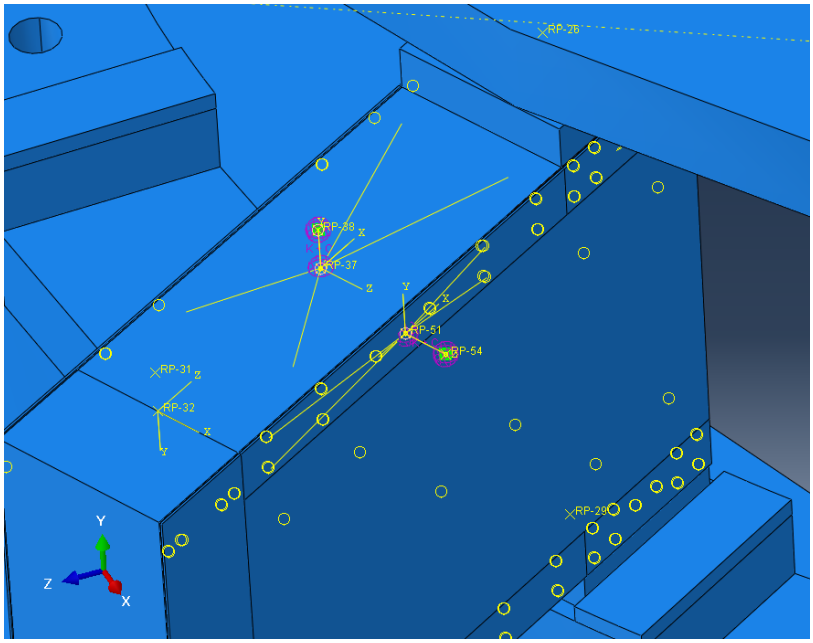

Figure 3.24 Location of TVA Tuned at 1335 Hz and 1097.5 Hz

Table 3.16 Transmissibility Comparison of Without TVA, P8+P10, P8+P10+P16 and P8+P16 in Lateral Direction

	Lateral Transmissiblity at Resonance Frequency				
	Peak at 506 Hz	**Peak at 529 Hz**	**Peak at 1097.5 Hz**	**Peak at 1338 Hz**	**Peak at 1554 Hz**
Without TVA	1.126	0.965	0.134	0.114	0.523
P8+P10	0.207	0.632	0.338	0.0221	0.532
P8+P10+P16	0.115	0.779	0.244	0.0169	0.386
P8+P16	0.194	0.7696	0.107	0.0286	0.493

Upon reviewing the outcomes presented in Table 3.16, it is apparent that the most reasonable strategy involves the implementation of double TVA system. In other words, tuning one TVA at 1335 Hz in the axial direction and the other at 1097 Hz for lateral direction appears to be the most efficacious approach, which are seen in Figure 3.24. Hence, parametric study of the structure with the utilization of double TVA tuned at 1335 Hz and 1097.5 Hz has been conducted, and the results are presented in Table 3.17.

Table 3.17 Double TVA Parametric Results in Lateral Direction

	Lateral Transmissiblity at Resonance Frequency				
	Peak at 506 Hz	**Peak at 529 Hz**	**Peak at 1097.5 Hz**	**Peak at 1338 Hz**	**Peak at 1554 Hz**
Without TVA	1.126	0.965	0.134	0.114	0.523
P8+P10+P14	0.270	0.690	0.2592	0.0479	0.6082
P8+P10+P16	0.194	0.7696	0.107	0.0286	0.493
P8+P10+P17	0.166	0.807	0.0546	0.0227	0.4575
P8+P10+P18	0.145	0.834	0.0325	0.0189	0.444

As a result, the configuration of 45 grams TVA tuned at 1335 Hz in the axial direction combined with 25 grams TVA tuned at 1097.5 Hz in the lateral direction has been chosen. The axial and lateral transmissibility values for these results are presented in Table 3.18 and Table 3.19. Moreover, transmissibility results are plotted together for the situation without TVA and with TVA implemented in Figure 3.25 and Figure 3.26.

Table 3.18 Transmissibility Comparison of Without TVA and with Double TVA in Axial Direction

	Axial Transmissiblity at Resonance Frequency		
	Peak at 1335 Hz	**Peak at 1610 Hz**	**Peak at 1800 Hz**
Without TVA	0.224	0.146	0.5857
Double TVA 1335 & 1097.5 Hz	0.0451	0.117	0.337

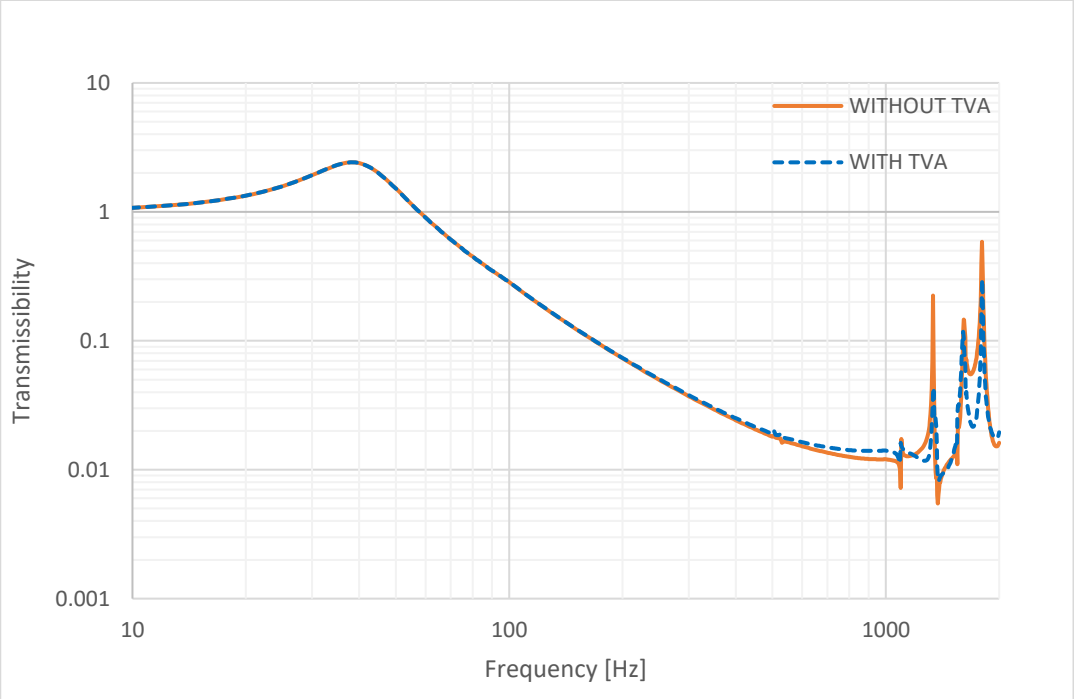

Figure 3.25 Transmissibility Comparison Plot for Double TVA in Axial Direction

Table 3.19 Transmissibility Comparison of Without TVA and with Double TVA in Lateral Direction

	Lateral Transmissiblity at Resonance Frequency				
	Peak at 506 Hz	**Peak at 529 Hz**	**Peak at 1097.5 Hz**	**Peak at 1338 Hz**	**Peak at 1554 Hz**
Without TVA	1.126	0.965	0.134	0.114	0.523
Double TVA 1335 & 1097.5 Hz	0.166	0.807	0.0546	0.0227	0.4575

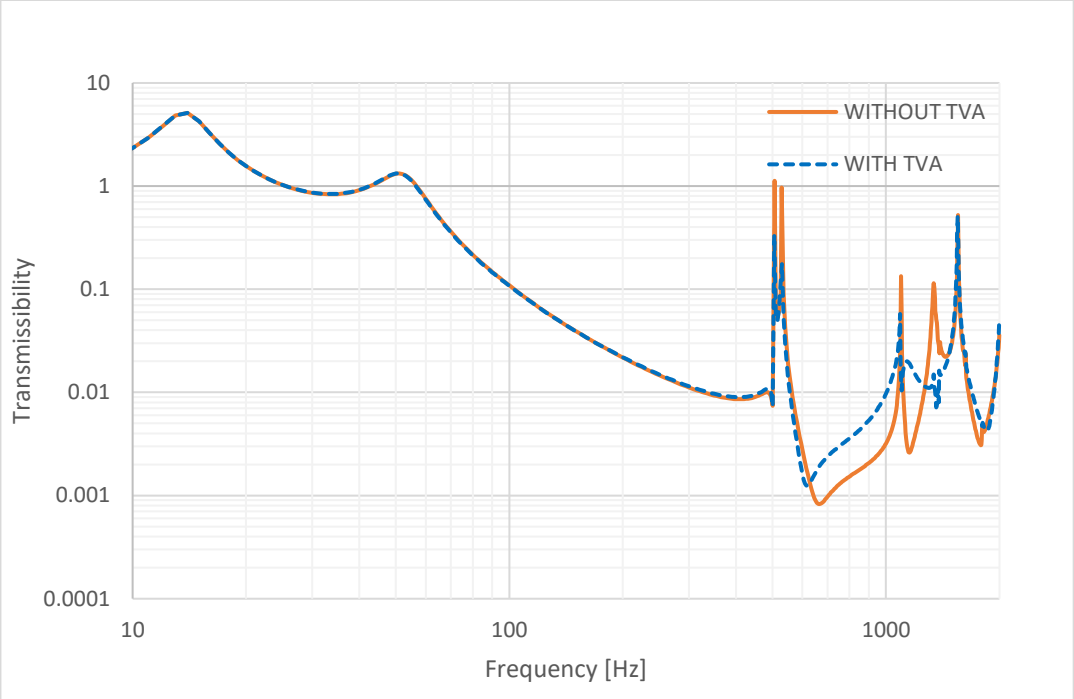

Figure 3.26 Transmissibility Comparison Plot for Double TVA in Lateral Direction

3.3 Target Mode Determination

Upon examining the results of the implementation of TVA to the previous triple isolator test configuration, it can be observed that the TVA concept is feasible and effective. In this section, the examination of vibration isolation system consisting of

60 isolators and the subsequent scaling to eliminate asymmetry and create a configuration where all TVAs can be equally excited is undertaken to establish a proof of concept TVA test structure. This initiative is prompted by the fact that asymmetry is not apparent in the vibration isolation system consisting of 60 isolators, and there is a need to ensure equal excitation of all TVAs both in axial and lateral directions. Firstly, the mode shapes of the vibration isolation system consisting of 60 isolators have been examined by defining the payload as a point mass. The material property of the VEM layers has been set with Young's Modulus value at 1000 Hz, and their mass densities have been chosen to be very small to eliminate undesired mode shapes. The base holes of the isolators have been fixed as BC.

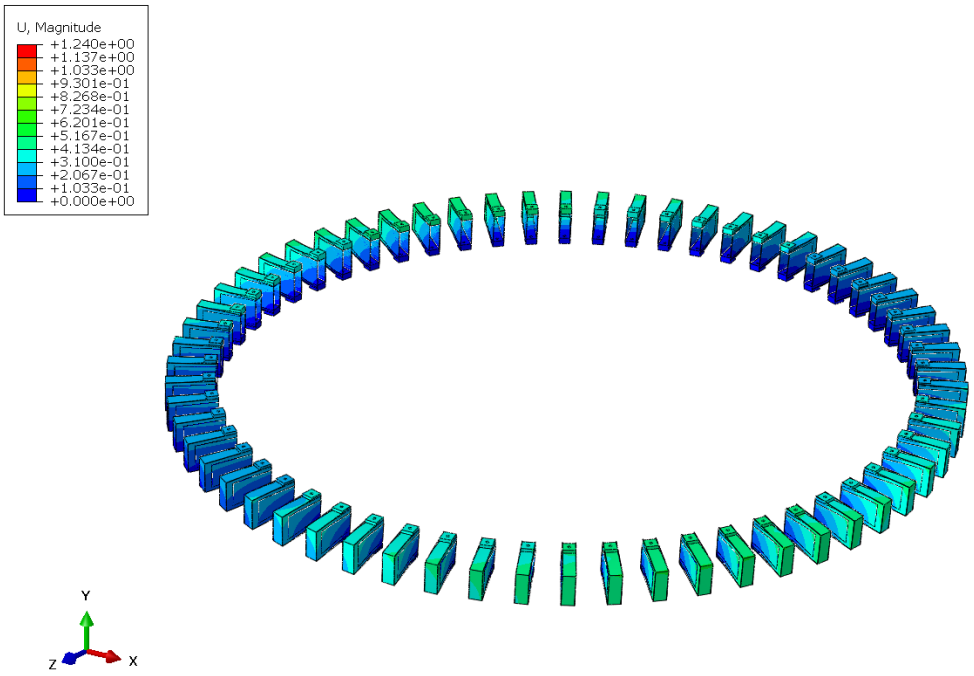

Figure 3.27 Rocking Mode Shape of Isolation System, 14 Hz

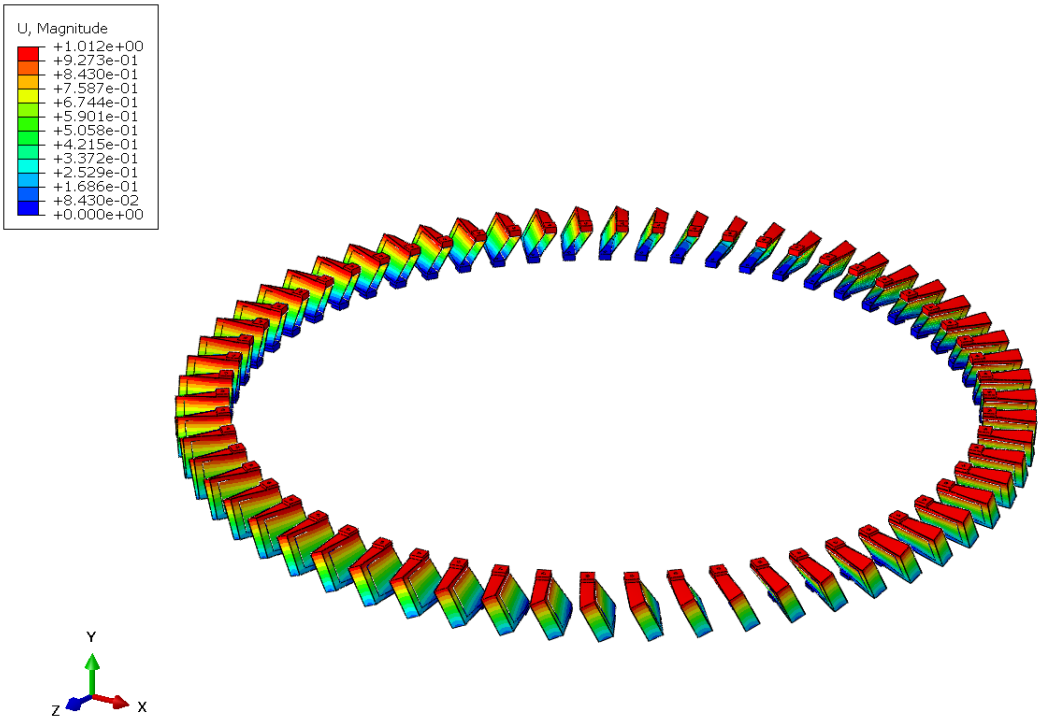

Figure 3.28 Torsional Mode Shape of Isolation System, 18 Hz

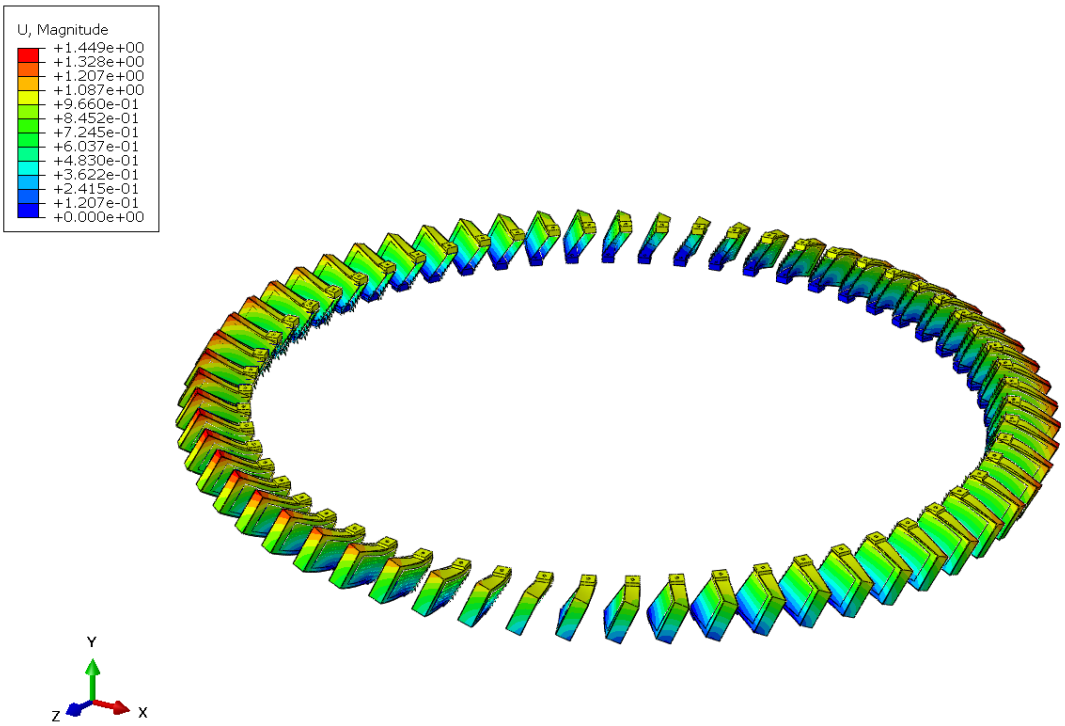

Figure 3.29 Lateral Mode Shape of Isolation System, 62 Hz

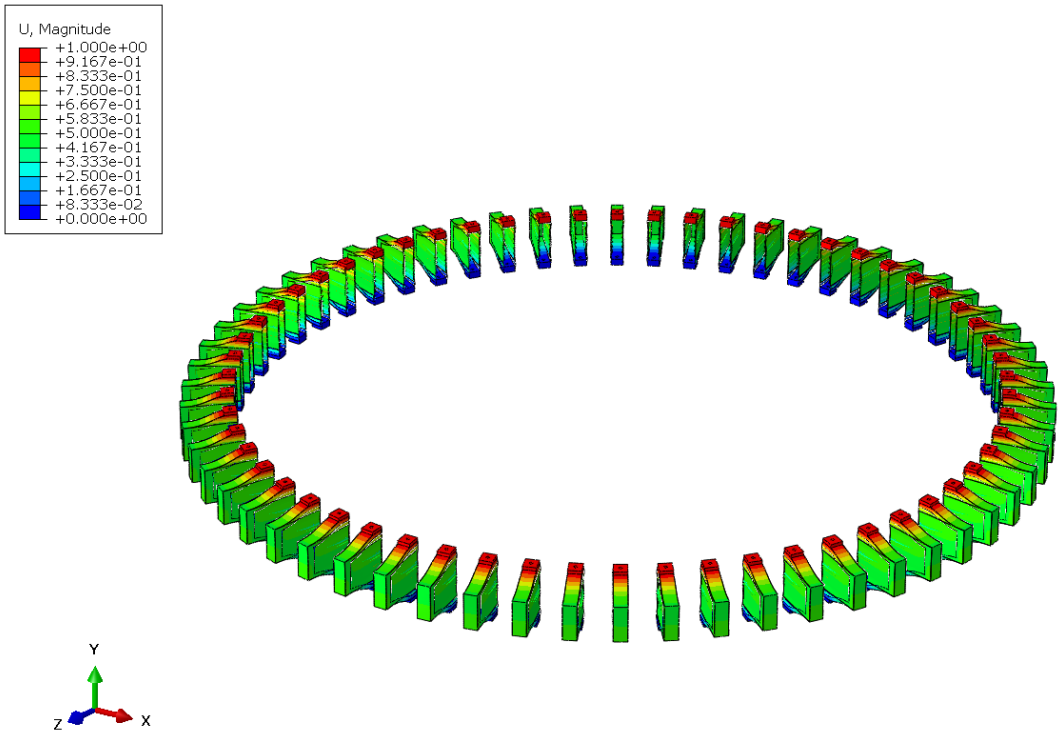

Figure 3.30 Axial Mode Shape of Isolation System, 83 Hz

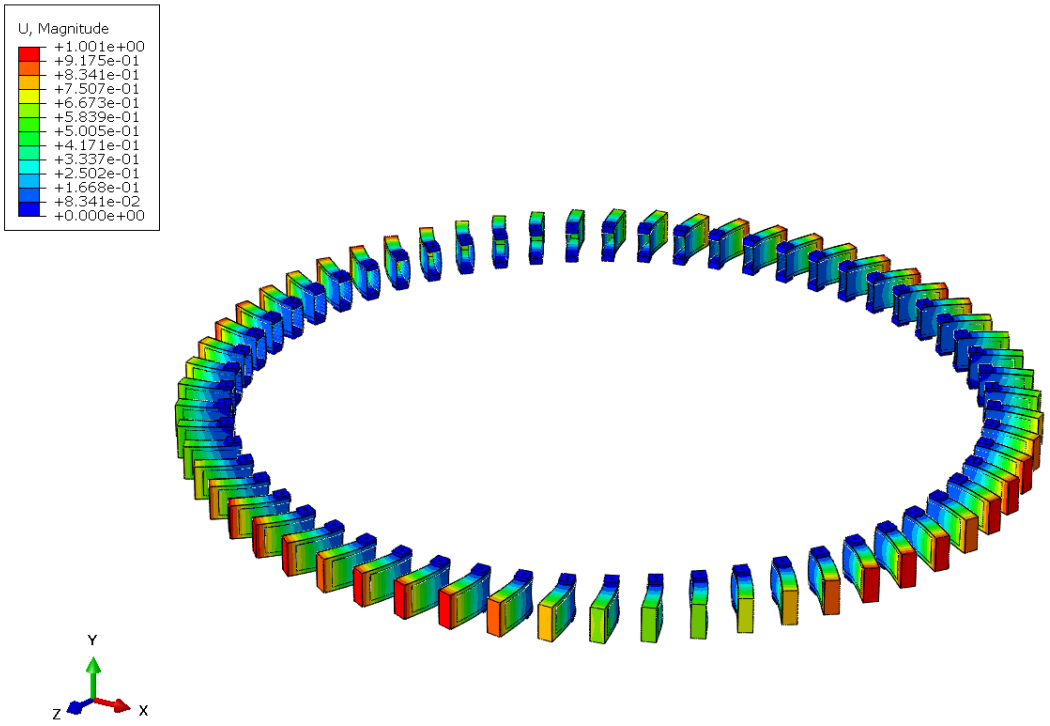

Figure 3.31 Internal Resonance of Isolators, 1479 Hz

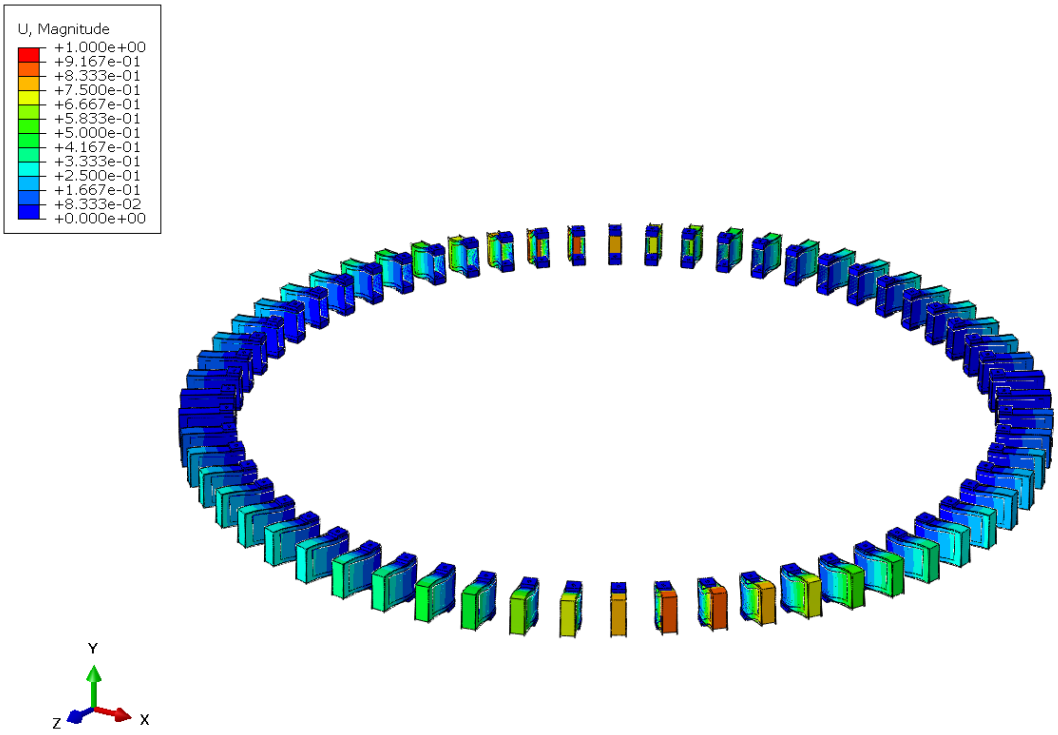

Figure 3.32 Internal Resonance of Isolators, 1693 Hz

Upon examining the mode shapes shown in Figure 3.27 to Figure 3.32, it is obvious that only the internal resonances of the isolators occur at high frequencies. The frequencies of the isolation system manifest at lower levels. Specifically, the lateral internal resonance of the isolators is observed at 1479 Hz, while the axial internal resonance occurs at 1693 Hz. Transmissibility plots for the axial and lateral directions of the vibration isolation system consisting of 60 isolators is obtained to observe whether peaks occur in the transmissibility values during these internal resonances of isolators. Unit amplitude sin wave is subsequently exerted to fixture holes over the relevant frequency range as an input to FEA software. It has to be noted that other directions are fixed apart from sin wave is applied as BC. ABAQUS analysis involves the utilization of the "Steady-state dynamics, Direct" step, which is appropriate for specifying frequency-dependent viscoelastic properties. Then, transmissibility values are calculated by dividing the accelerations at the reference point where the point mass is added by the accelerations at the base hole center of the isolators. The obtained results are shown in Figure 3.33 and Figure 3.34.

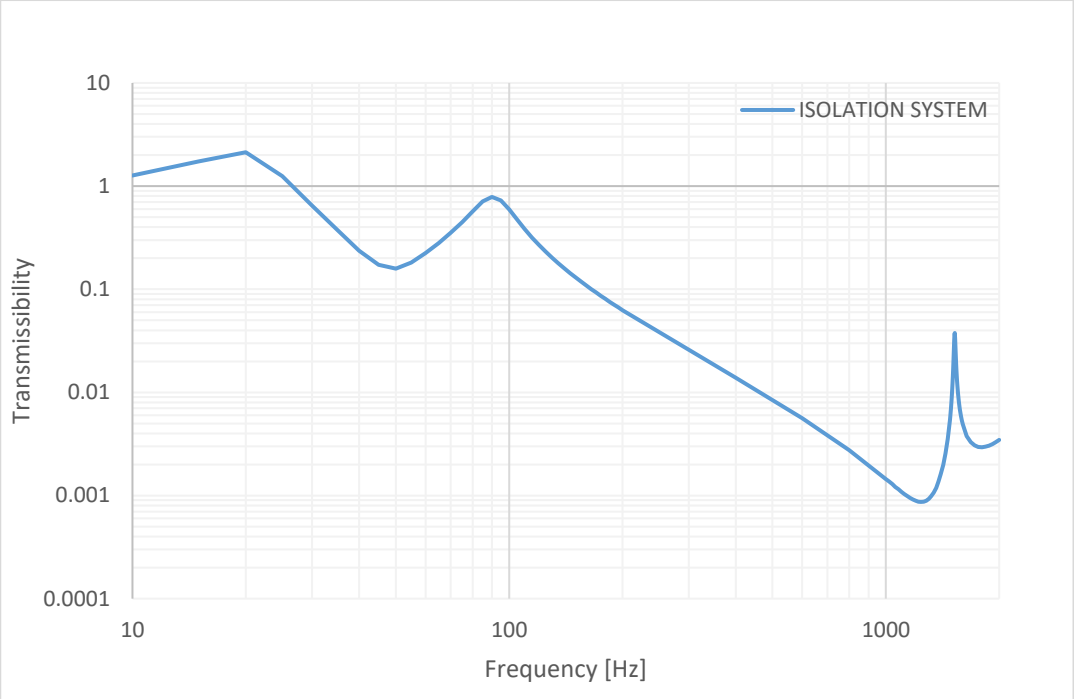

Figure 3.33 Transmissibility Plot in Axial Direction for Isolation System

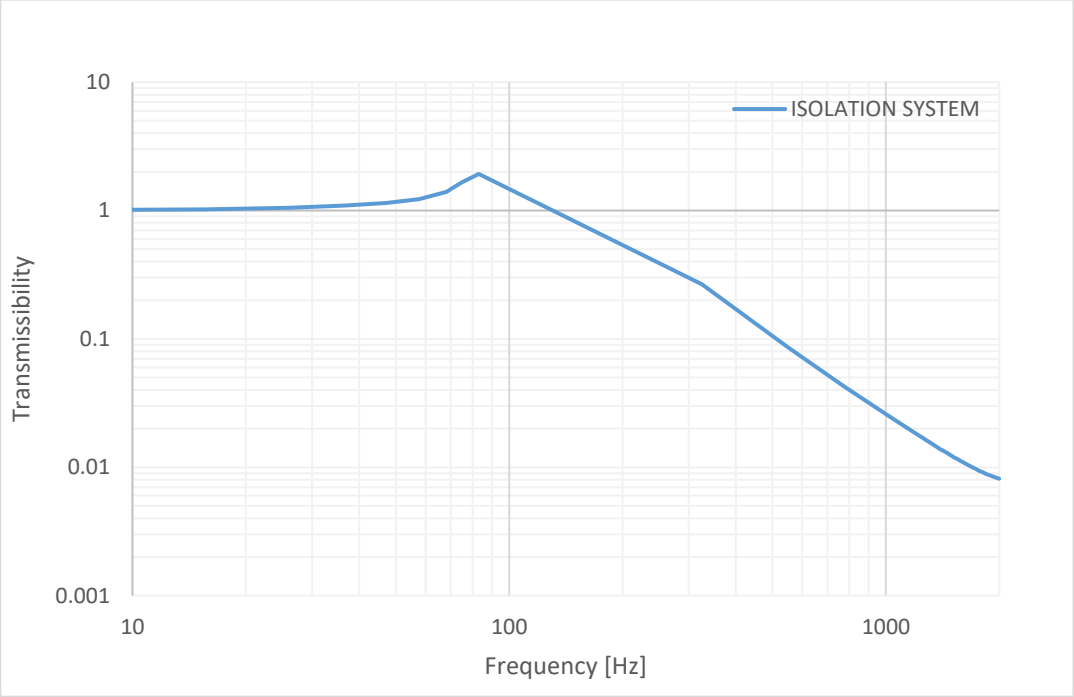

Figure 3.34 Transmissibility Plot in Lateral Direction for Isolation System

Looking at these plots, one does not observe any peak in the axial direction at high frequencies. However, a peak is observed at approximately 1500 Hz in the lateral direction. When examining the mode shape where this peak occurs, it is observed that the isolators undergo lateral rotational motion while the payload remains stationary, indicating rigid behavior. TVAs are implemented at this frequency to enhance damping. Since verification with testing is necessary, it is required to scale the vibration isolation system consisting of 60 isolators by maintaining the resonant frequency and mode shape for further experimentation.

Quadruple test configuration in an X shape is planned to make the payload as rigid as possible and equally excite all isolators. Initially, a cylindrical payload made of steel with a diameter of 120 mm and a height of 75 mm is designed to fit the test fixture. Upon examining the frequency and mode shapes of the quadruple isolators and payload structure, it is observed that the configuration exhibits compatibility with the vibration isolation system consisting of 60 isolators. The mode shapes and resonance frequencies of the quadruple test configuration are illustrated in Figure 3.35 to Figure 3.39. Similarly to the vibration isolation system consisting of 60 isolators, the isolators in quadruple test configuration exhibit lateral rotational motion while the payload remains rigid at the resonance point observed at nearly 1400 Hz.

Unit amplitude sin wave is subsequently exerted to fixture holes over the relevant frequency range as an input to FEA software. It has to be noted that other directions are fixed apart from sin wave is applied as BC. ABAQUS analysis involves the utilization of the "Steady-state dynamics, Direct" step, which is appropriate for specifying frequency-dependent viscoelastic properties. Then, transmissibility values are calculated by dividing the accelerations at the reference point added to the middle of the top surface of a payload by the accelerations at the base hole center of the isolators. The obtained transmissibility result for the quadruple test configuration is shown in Figure 3.40.

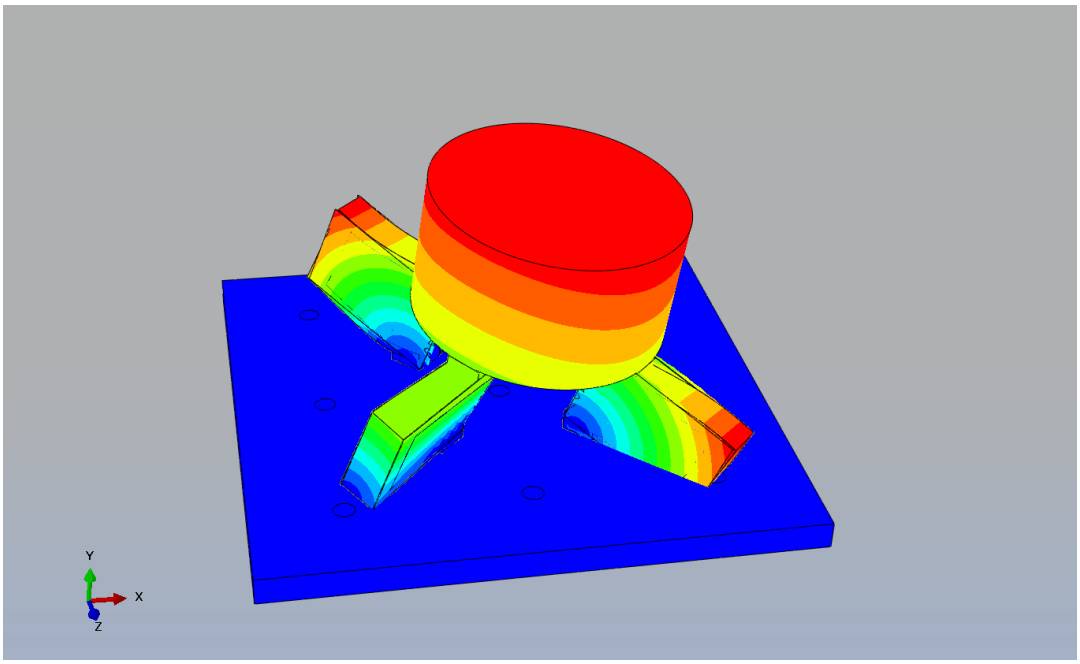

Figure 3.35 Rocking Mode Shape of Quadruple Test Configuration, 62 Hz

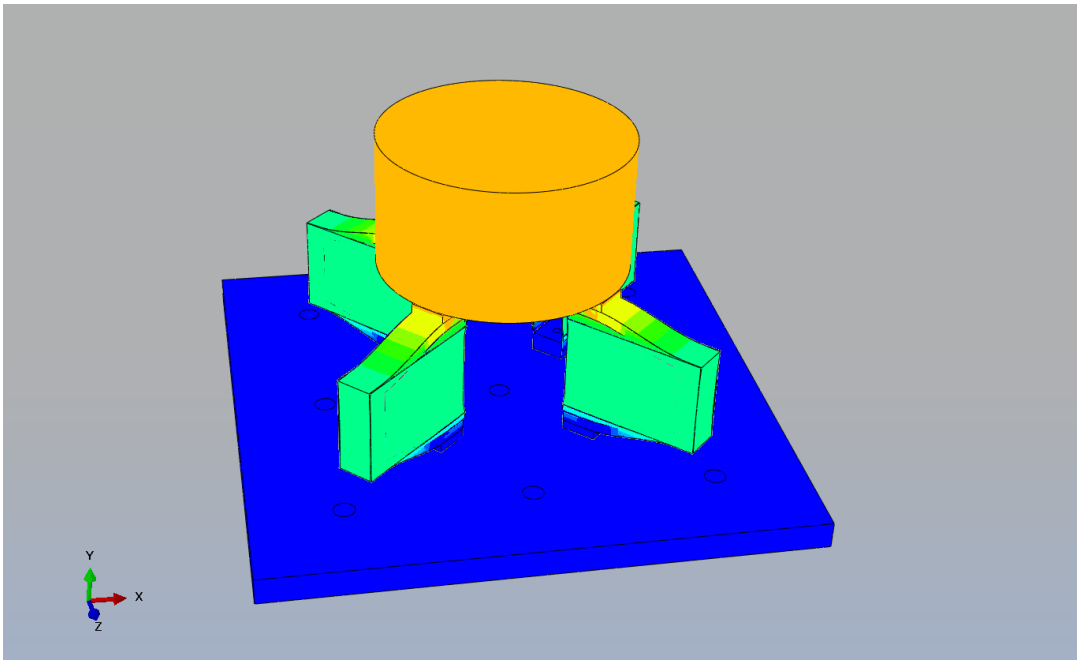

Figure 3.36 Axial Mode Shape of Quadruple Test Configuration, 137 Hz

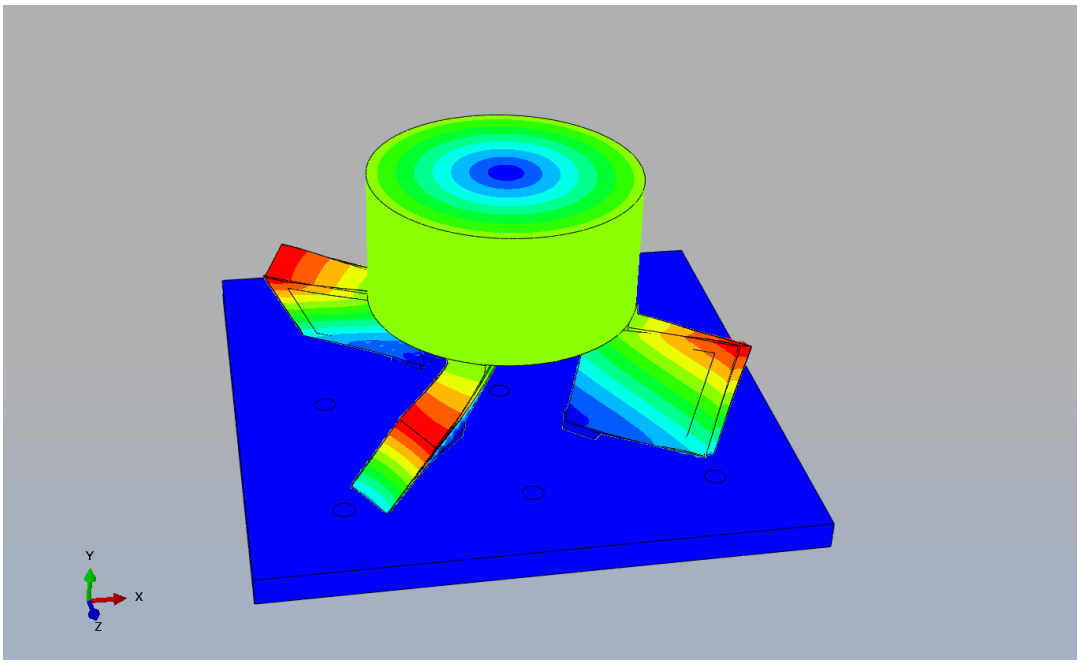

Figure 3.37 Torsional Mode Shape of Quadruple Test Configuration, 153 Hz

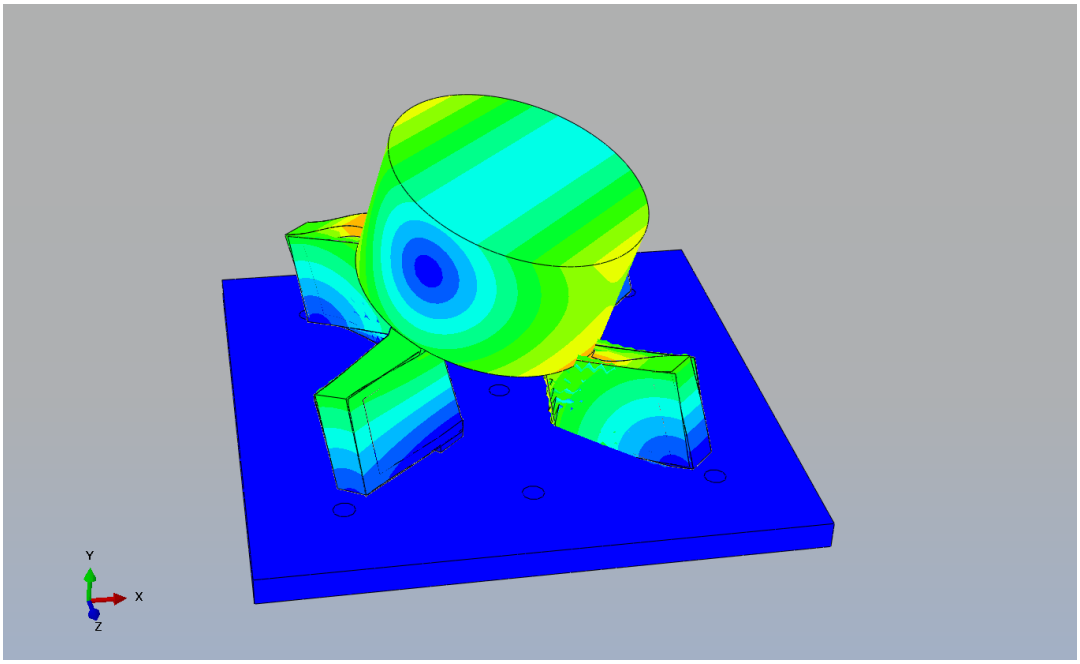

Figure 3.38 Lateral Mode Shape of Quadruple Test Configuration, 231 Hz

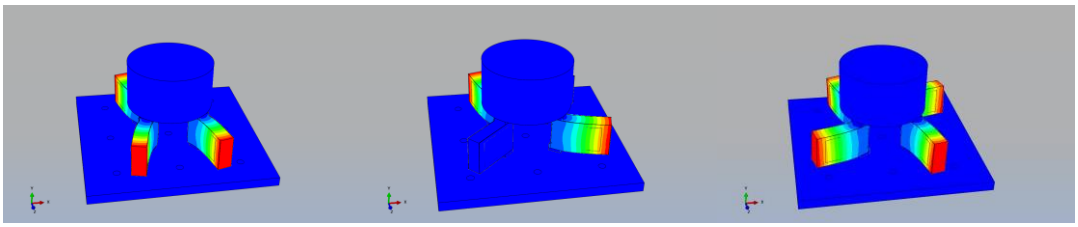

Figure 3.39 Internal Resonances of Isolators: 1389 Hz, 1410 Hz, 1440 Hz

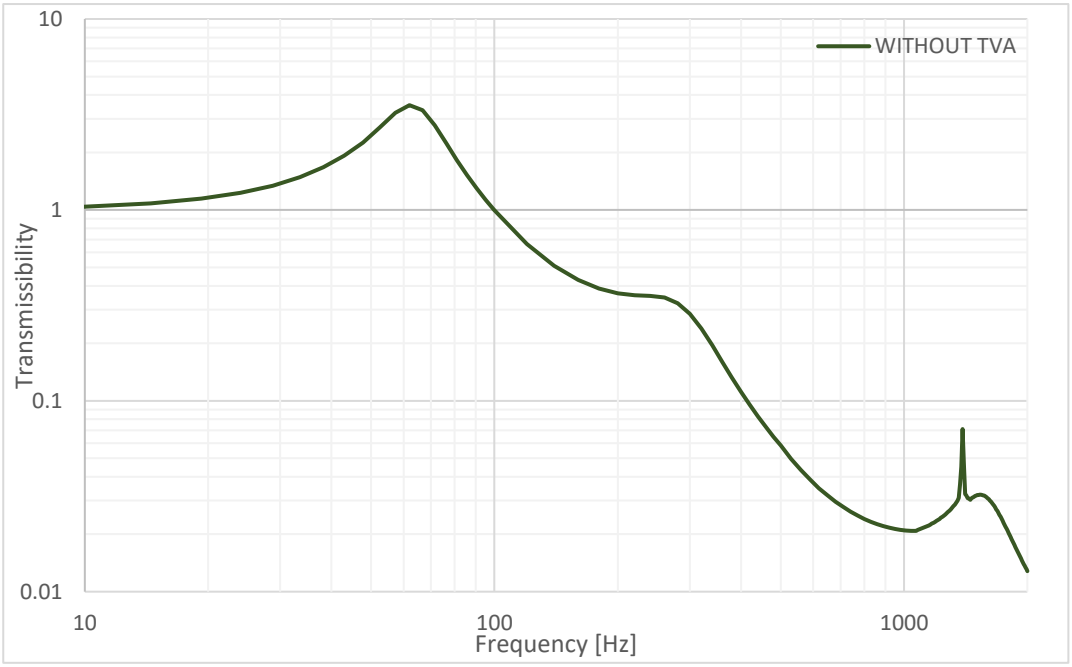

Figure 3.40 Transmissibility Plot in Lateral Direction for Quadruple Test Configuration

CHAPTER 4

PROOF OF CONCEPT

In this chapter, the implementation of the TVA concept is validated on the quadruple test structure through theoretical and physical design. After completing the TVA design, the obtained transmissibility values from the finite element analysis software are compared with the transmissibility values obtained from the random vibration test to demonstrate the alignment of the model with the actual test structure. In this way, the proof of the TVA usage concept is completed.

4.1 TVA Design Theoretically

Firstly, the TVA design is parametrically implemented using a mass-spring-dashpot structure again as mentioned in the previous chapter. The target frequency is determined as 1389 Hz referring to Figure 3.34 for this parametric study. The isolators exhibit lateral rotational motion at that resonance point of 1389 Hz. Therefore, TVAs are placed on the outer middle part of the lateral surface of the each isolators as shown in Figure 4.1.

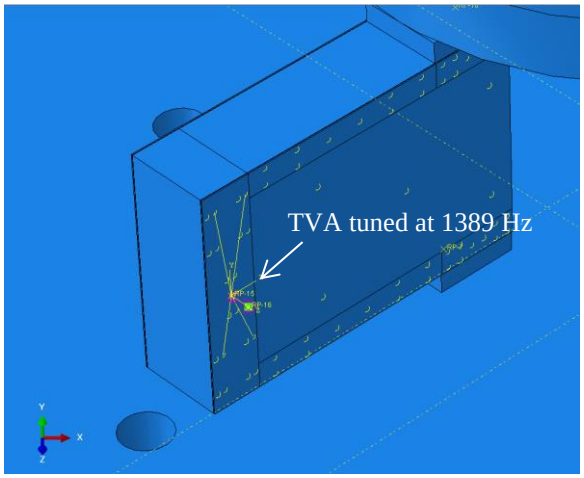

Figure 4.1 Location of TVA Tuned at 1389 Hz

The parameter information for TVAs tuned to 1389 Hz for different masses are shown in Table 4.1. ABAQUS uses Newton-Tonne-mm unit system. Therefore, the units of the parameters in Table 4.1 have been adjusted accordingly to this system.

Table 4.1 TVA Parameters for 1389 Hz

	Mass [Tonne]	**Spring Stiffness [N/mm]**	**Dashpot Coefficient [N.s/mm]**	**Damping Ratio**
Q1	0.000003	329.2719	0.031429	0.5
Q2	0.000006	658.5438	0.062859	0.5
Q3	0.000010	1097.573	0.104765	0.5

During the parametric study, the mass is added as a point mass and constrained with spring-dashpot. Point mass is coupled with spring-dashpot, and only allowed to move in the direction perpendicular to the constrained surface. Reference points are added to the point mass location and the spring location on the surface of the isolator. Then, these reference points are linked to each other and the surface through a "coupling" constraint type in ABAQUS.

Unit amplitude sin wave is subsequently exerted to fixture holes over the relevant frequency range. It has to be noted that other directions are fixed apart from sin wave is applied as BC. ABAQUS analysis involves the utilization of the "Steady-state dynamics, Direct" step, which is appropriate for specifying frequency-dependent viscoelastic properties. Therefore, transmissibility results are obtained by using "Steady-state dynamics, Direct" step,

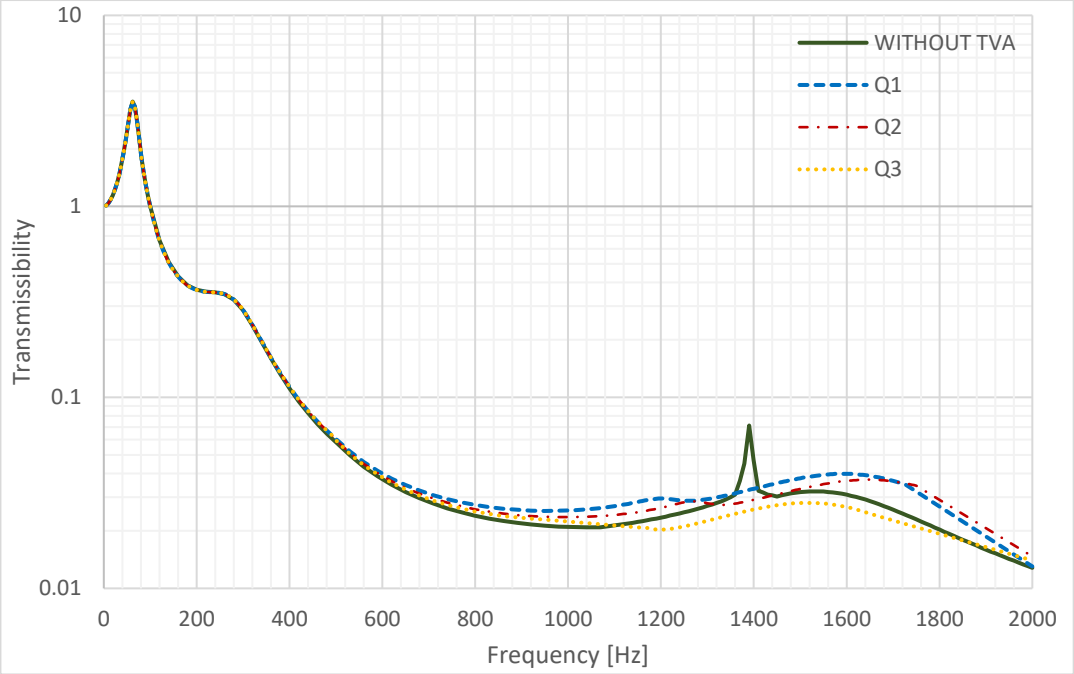

Figure 4.2 Parametric Transmissibility Comparison of TVAs Tuned at 1389 Hz

The improvement increases as the mass increases, but it causes deterioration beyond a certain point especially towards 2000 Hz by looking the results shown in Figure 4.2. Therefore, the best option is to use Q3.

4.2 TVA Design Physically

The parametrically designed TVA needs to be physically obtained to be utilized in the labarotary vibration tests. Therefore, TVA corresponding to Q3 parameter set has been geometrically obtained in this section.

For the current investigation, a viscoelastic material with a high damping capability at higher frrequencies like 1000 Hz has been chosen from the market. Specifically, 3M-468 MP which is a double-sided adhesive transfer tape with a thickness of 0.12 mm has been selected. The dynamic properties of 3M-467 MP were determined using the nomogram given in Figure 4.3. Firstly, a horizontal line is drawn from the desired operating frequency to employ the nomogram. Then, the intersection of this horizontal line with the constant working temperature line is identified, and room

temperature is considered as the working temperature. Later on, a vertical line is then drawn from the marked point, and the points where this vertical line intersects with the complex modulus of elasticity curve and the loss factor curve indicate the values of the material properties at hat frequency. Poisson ratio is taken as an average value of 0.35.

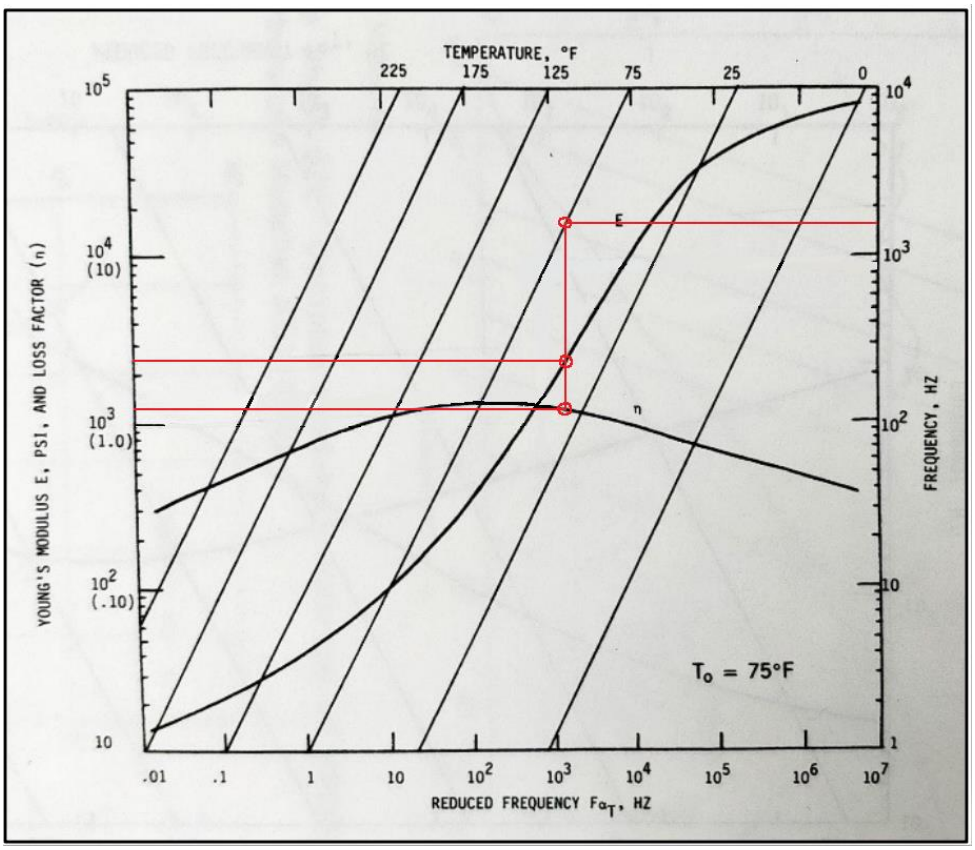

Figure 4.3 Nomogram of 3M-468 MP [28]

Loss factor and storage modulus values are required to define the material in ANSYS software. Therefore, the complex modulus of elasticity obtained from the nomogram has been used with Equation (4.1) and (4.2) to determine these values.

$$\eta = \frac{E''}{E'} \tag{4.1}$$

$$E = E' + iE'' \tag{4.2}$$

Where η denotes loss factor, i denotes complex number, E' denotes storage modulus, E'' denotes loss modulus and E denotes complex modulus of elasticity. The material properties of the 3M-468 MP defined in ANSYS software are shown in Figure 4.4.

	Property	Value	Unit
2	Material Field Variables	Table	
3	Density	1012	kg m^-3
4	Material Dependent Damping		
5	Damping Ratio	0,5	
6	Constant Structural Damping Coefficient	= 1	
7	Isotropic Elasticity		
8	Derive from	Young's Modulus and Poisson...	
9	Young's Modulus	9,7507E+06	Pa
10	Poisson's Ratio	0,35	
11	Bulk Modulus	1,0834E+07	Pa
12	Shear Modulus	3,6114E+06	Pa

Figure 4.4 Material Definition of 3M-468 MP in ANSYS

The geometric model of the TVA has been obtained by doing some iterations on the geometric parameters. The damped frequency of the geometrically designed TVA is calculated as 1400 Hz in ANSYS as shown in Figure 4.5.

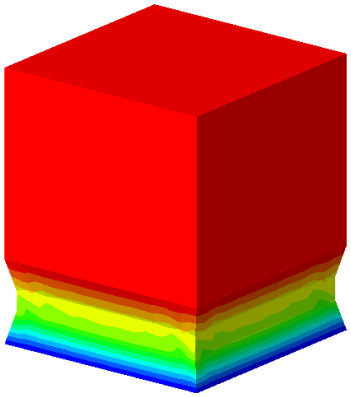

Figure 4.5 Geometrical Representation of TVA

As a result of the analyses, it has been determined that TVA should be made of 3M-468 MP material with a thickness of 3.1 mm and steel material with a thickness of 10 mm. Therefore, this means that lamination of 26 layers of 3M-468 MP are required for each TVA.

Frequency response function (FRF) plot of the reference point shown in Figure 4.6 has been determined to validate the geometrically obtained TVA. Harmonic unit

displacement has been applied as the input to this reference point for the analysis. The base of TVA has been fixed as a boundary condition for the analysis. The obtained direct point FRF is shown in Figure 4.7.

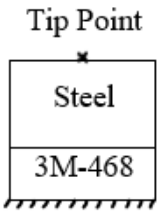

Figure 4.6 Schematic of TVA

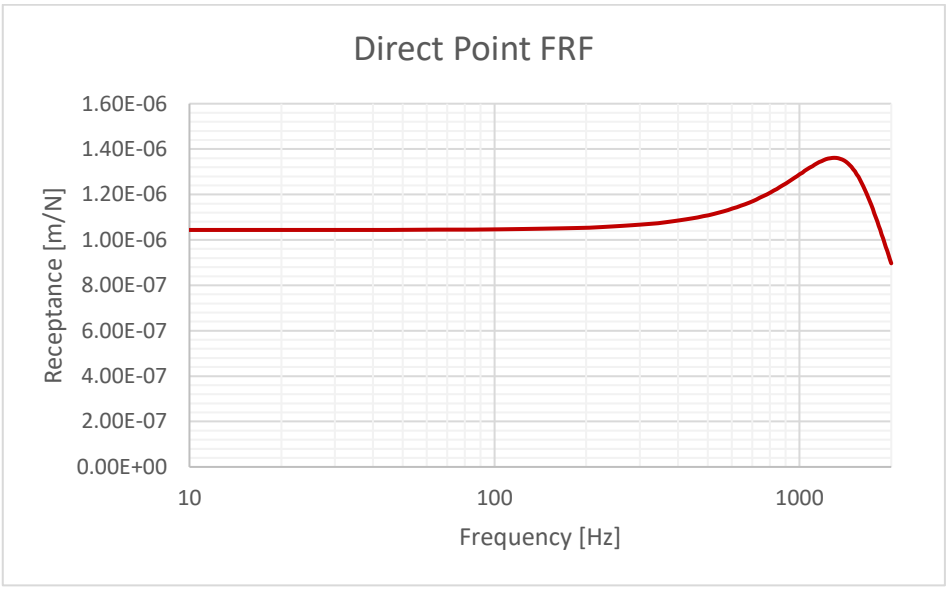

Figure 4.7 Direct Point FRF at the Tip Point of TVA

The manner in which TVAs connect to the quadruple test configuration and whether better results are achieved when they are placed directly on the VEM layers or cut and placed on an aluminum base were examined. The obtained results indicate that there is no issue with placing the TVAs directly on the VEM layers.

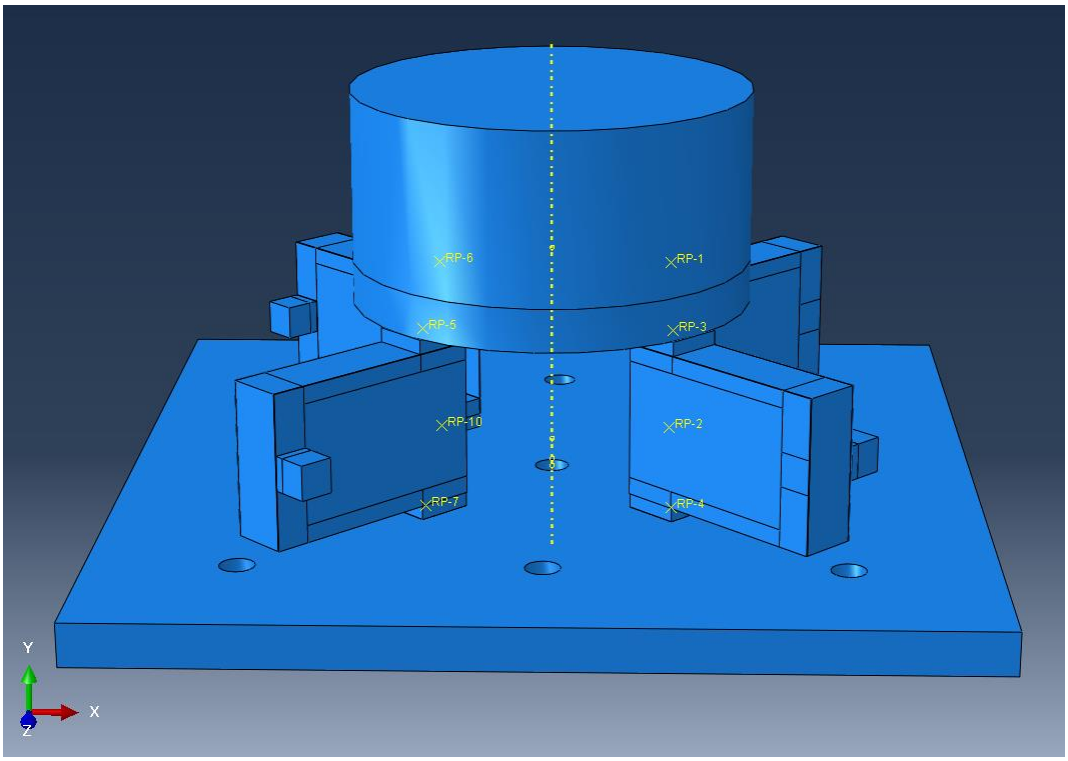

Figure 4.8 Quadruple Test Configuration with TVAs

TVAs are directly connected to the VEM layers using tie constraints in ABAQUS. Then, transmissibilities are tried to find with geometric TVA. Material properties of 3M-468 MP is defined in ABAQUS for some frequencies using the nomogram in Figure 4.3. Unit amplitude sin wave is subsequently exerted to fixture holes over the relevant frequency range in x-direction. It has to be noted that other directions are fixed apart from sin wave is applied as BC. ABAQUS analysis involves the utilization of the "Steady-state dynamics, Direct" step, which is appropriate for specifying frequency-dependent viscoelastic properties. The model of the test structure is shown in Figure 4.8, and the obtained transmissibility results are presented for comparison purposes. in Figure 4.9.

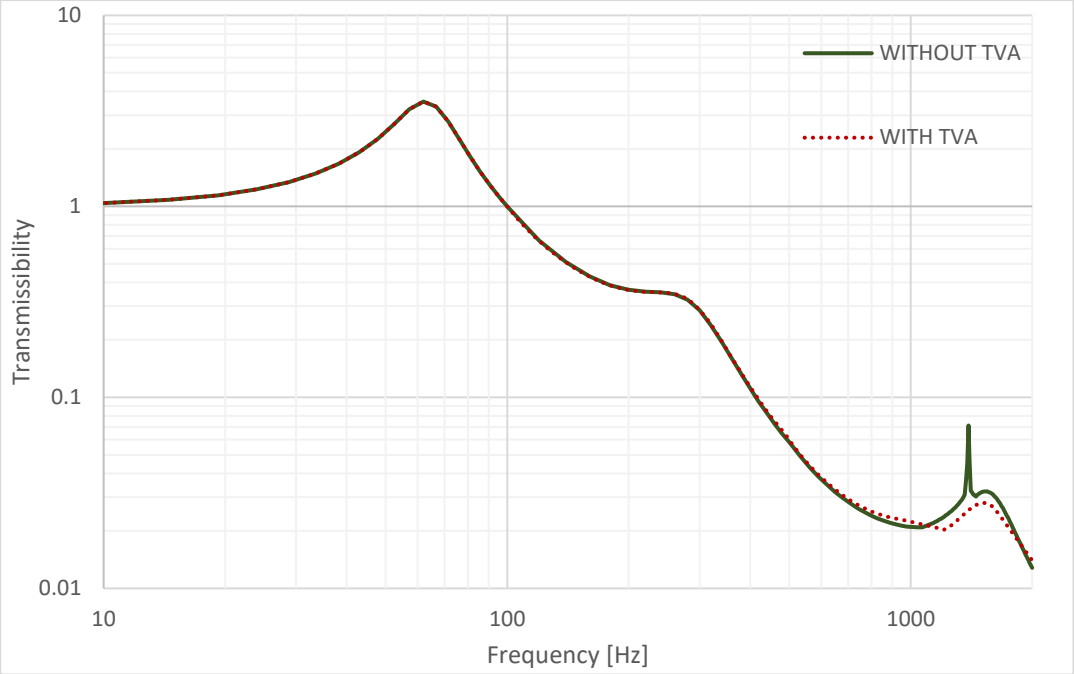

Figure 4.9 Transmissibility Comparison Plot in Lateral Direction for Quadruple Test Configuration

4.3 Test Procedure

Proof of the TVA concept has been performed via vibration tests in lateral direction. This section describes the preparations made before the test, the procedural steps performed during the test, and the findings obtained after the test.

The first step involves creating a list of necessary materials. The materials prepared before the test can be listed as follows:

- Four isolators made of aluminum 6061-T6
- Test adapter jig made of aluminum
- TVA base made of 3M-468 MP material, which is required for 26 layers of lamination for each TVA
- TVA load made of steel, which has 10 grams weight.

- Payload made of steel, which has 9 kg weight.
- VEM layers consisting of 50x82 mm ISD 112 polymer and stiffening aluminum layers

Simultaneously with the ongoing manufacturing of the required materials, the subsequent step involves the lamination process of TVA base. 26 layers of 3M-468 MP material has to be laminated separately for each TVA. It is necessary to be very careful during this process because water vapor must not be allowed to enter between the laminates. For this reason, each laminated layer was carefully prepared one by one. The resulting product is shown in Figure 4.10.

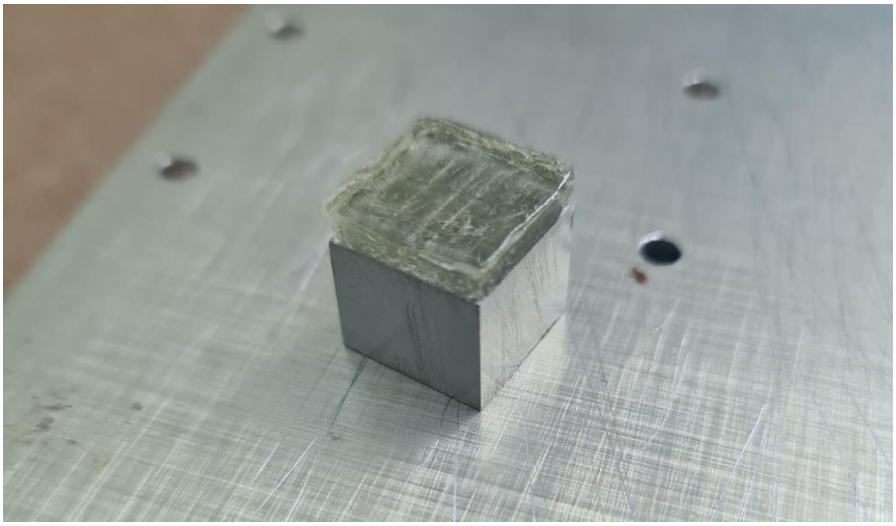

Figure 4.10 TVA Tuned at 1400 Hz

The third step involves determining the random input to be used in the tests. For this purpose, Minotaur-Payload random vibration environment during launch is taken from Minoator I User's Guide, and it is shown in Figure 4.11 [29]. It includes random vibration level between 20-2000 Hz.

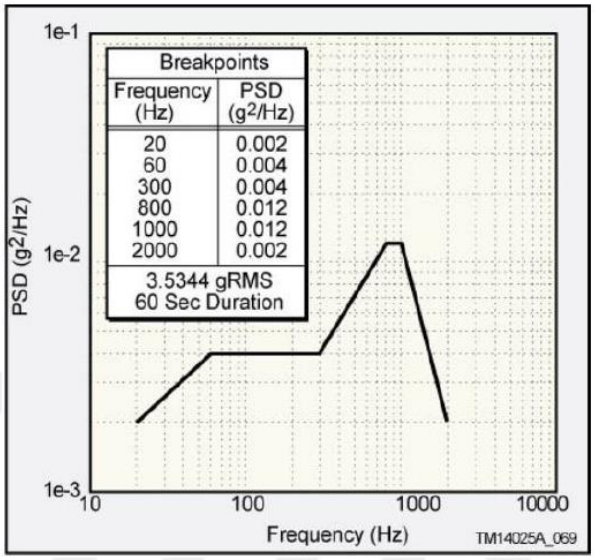

Figure 4.11 Vibration Environment of Minotaur-Payload During Launch [29]

Two separate tests were conducted. Initially, transmissibility values were measured for the quadruple test structure without TVA, and subsequently, after the implementatiın of TVA, transmissibility measurements were repeated. These measurements were taken at a specific point on the payload's tip and adapter jig to ensure compatibility with the locations used in the finite element analysis. The locations of the accelerometers are shown in Figure 4.12. Moreover, test setup is shown in Figure 4.13.

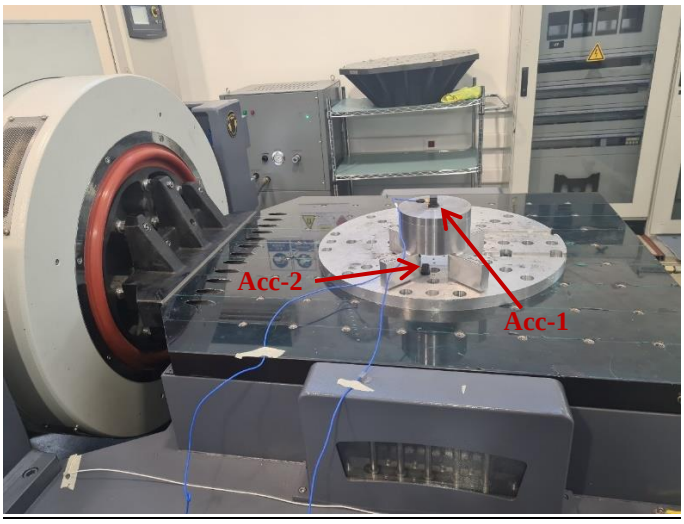

Figure 4.12 General View of Quadruple Test Structure Without TVA

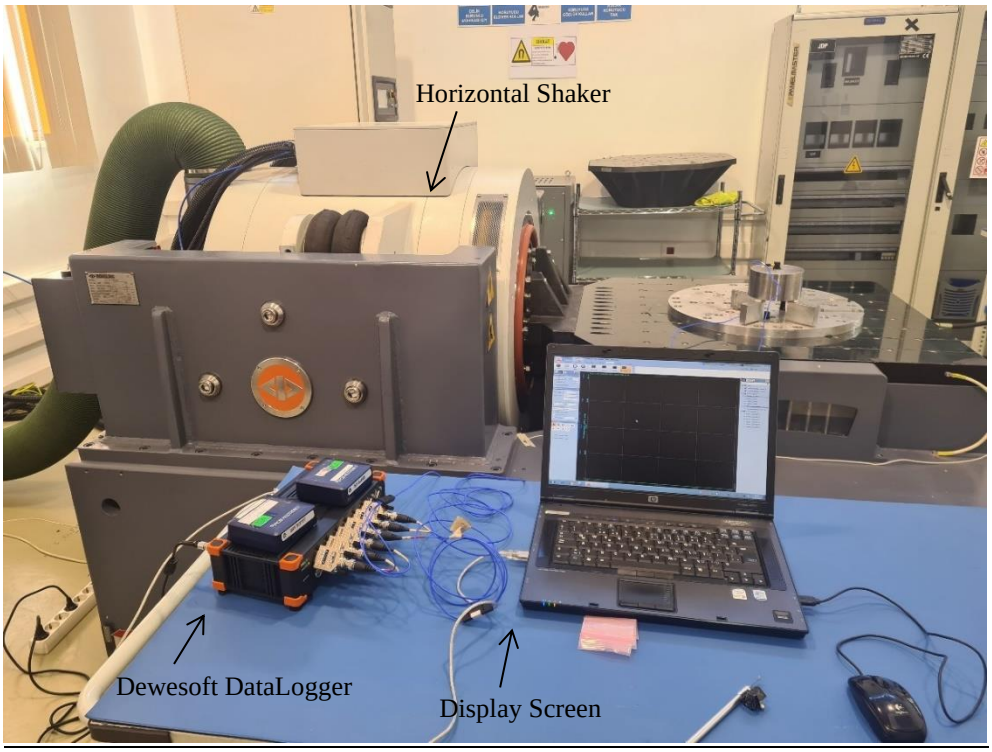

Figure 4.13 Experimental Setup for Vibration Testing

TVAs were immediately attached to the isolators after completing the lateral vibration test in the scenario without TVA as shown in Figure 4.14. Although it is recommended to wait for at least one day after this process the second test was conducted on the same day due to the availability of the vibration testing laboratory.

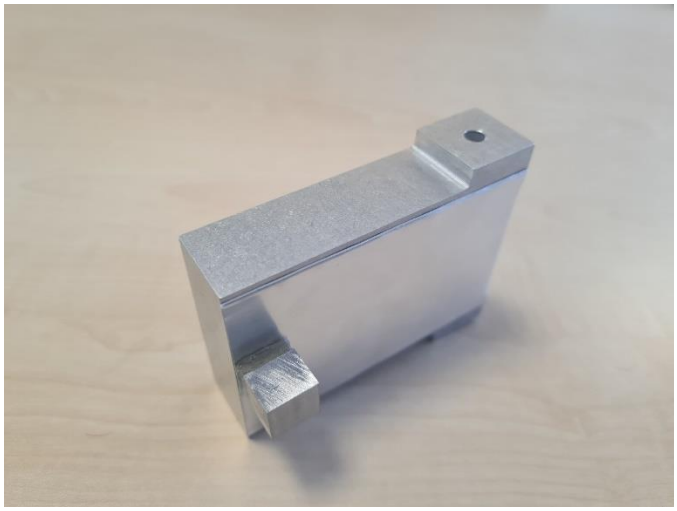

Figure 4.14 General View of One Isolator With TVA

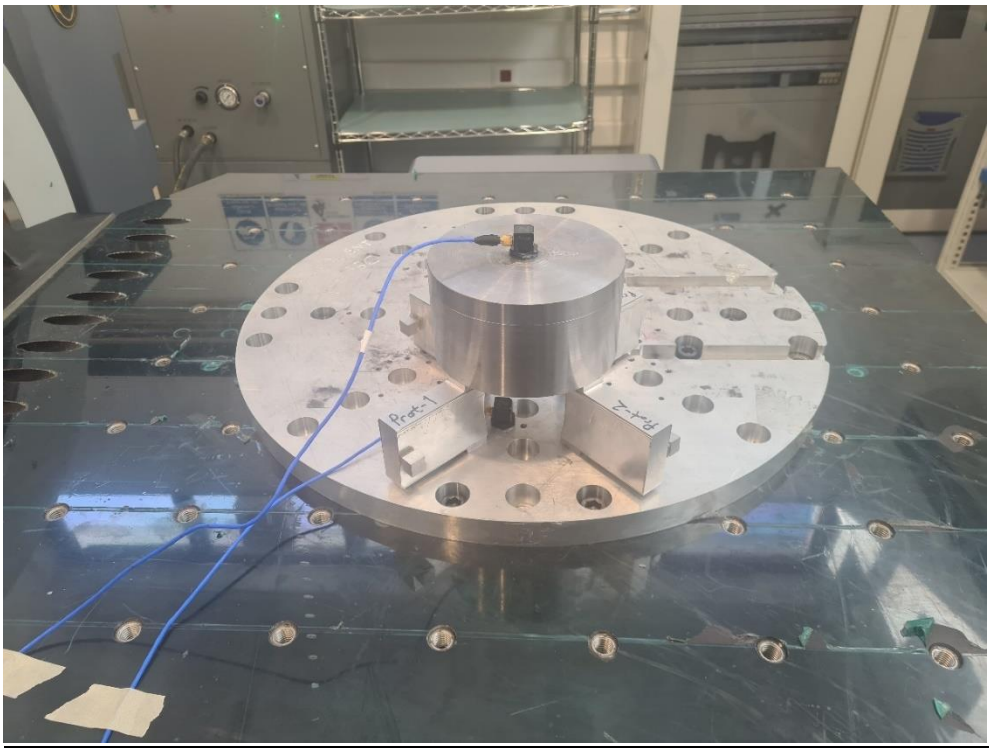

Figure 4.15 General View of Quadruple Test Structure With TVAs

General view of the test structure with TVAs is shown in Figure 4.15. Moreover, the test output includes transmissibility graphs and PSD responses. It is observed that the expected peak around 1400 Hz occurs around 1500 Hz upon examining the transmissibility plots. Similarly, there are some deviations in the frequencies of the isolation system. Moreover, it is observed that transmissibility value at internal resonance of the isolators has decreased from around 0.08 to 0.03 in Figure 4.16 and Figure 4.17. Therefore, it can be said that tests and analyses results are consistent with each other in terms of obtained improvement thanks to the use of TVAs.

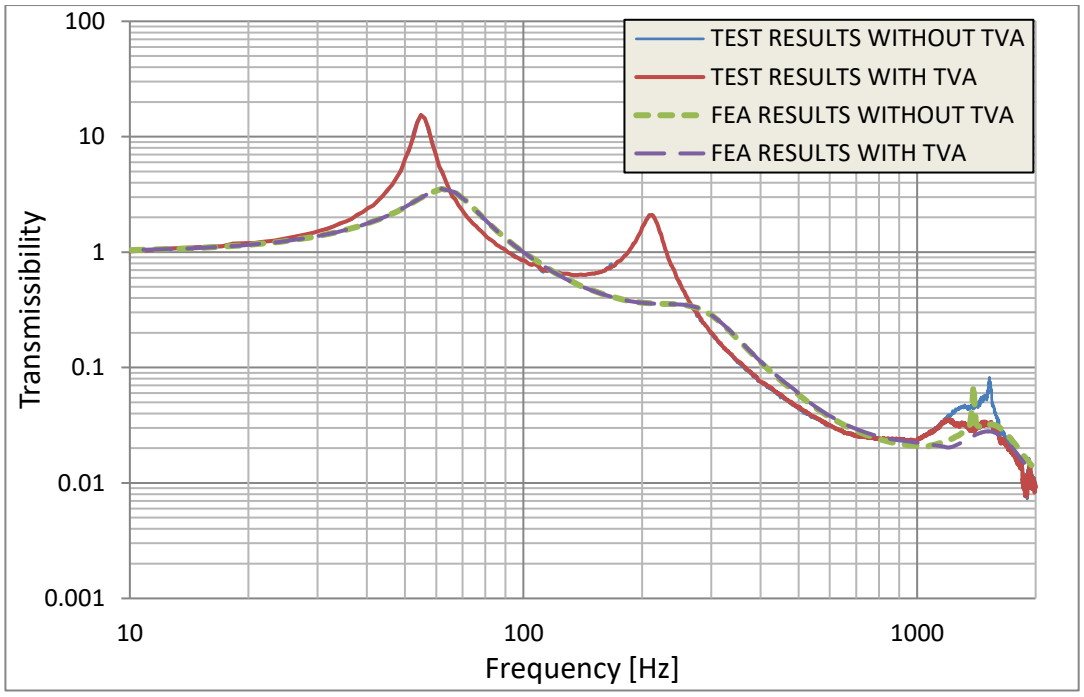

Figure 4.16 Random Vibration Test Comparison Plot in logx-logy Scale

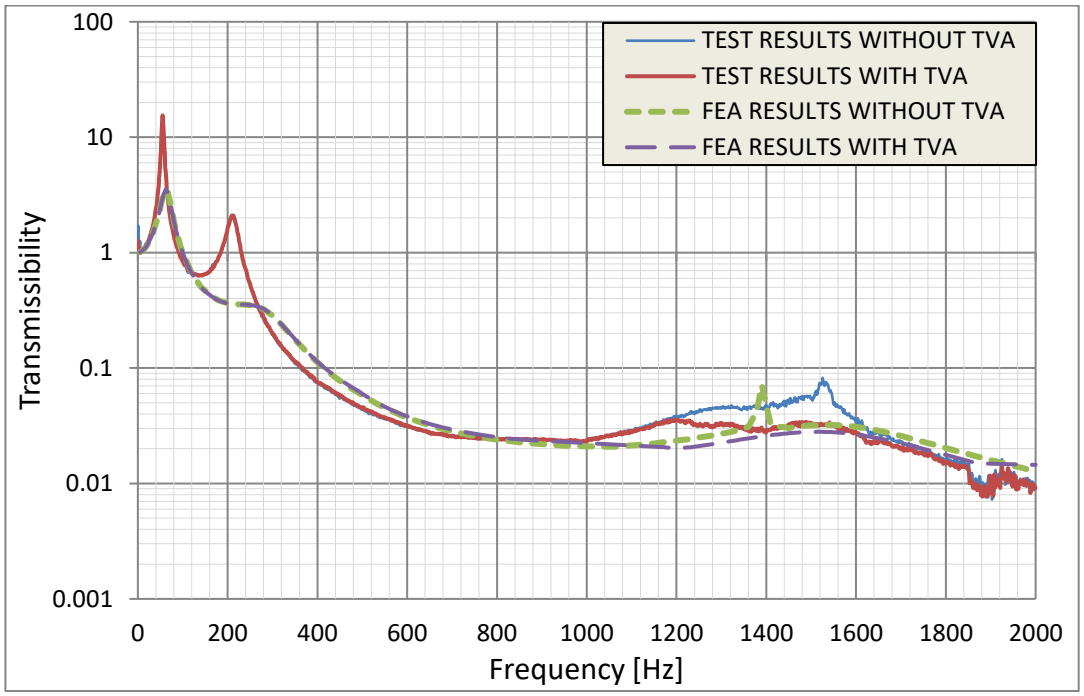

Figure 4.17 Random Vibration Test Comparison Plot in x-logy Scale

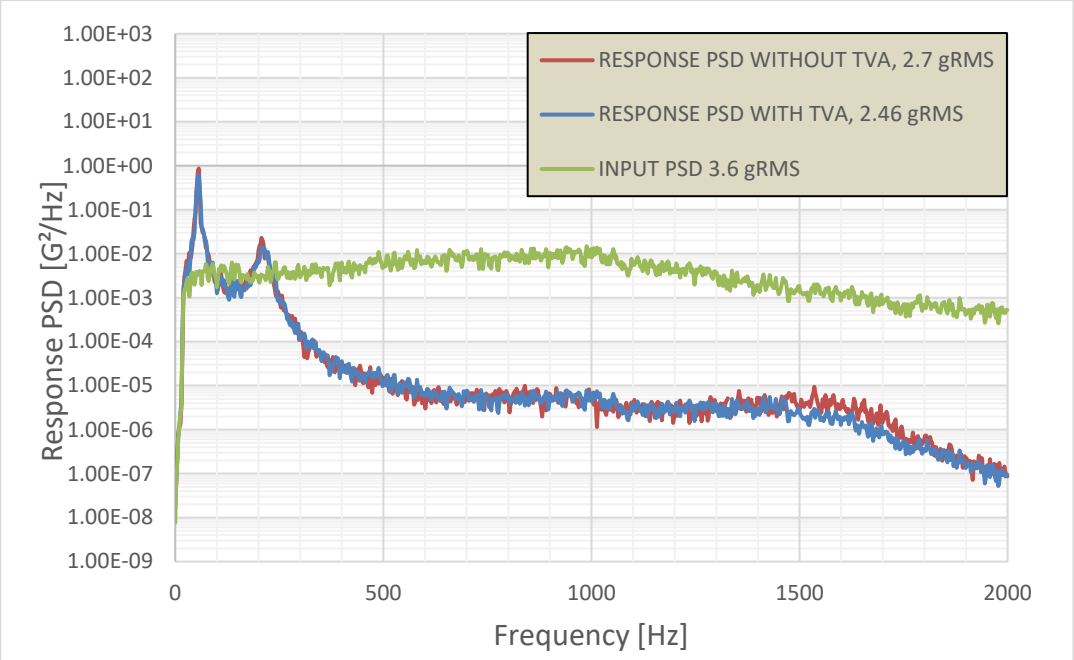

Figure 4.18 Response PSD Comparison Plot in x-logy Scale

Figure 4.18 displays the PSD responses of the isolation system against the PSD input. Response root mean square (RMS) accelerations results reveal the significant impact of TVA usage on the system.

CHAPTER 5

FATIGUE LIFE ESTIMATION

In this section, fatigue life analysis was conducted for the previously designed triple test structure, which had a failed vibration isolator named as T1. Subsequently, fatigue life analysis was also performed for quadruple test configuration with and without TVAs to compare the obtained results. The ANSYS fatigue tool is employed for this analyses.

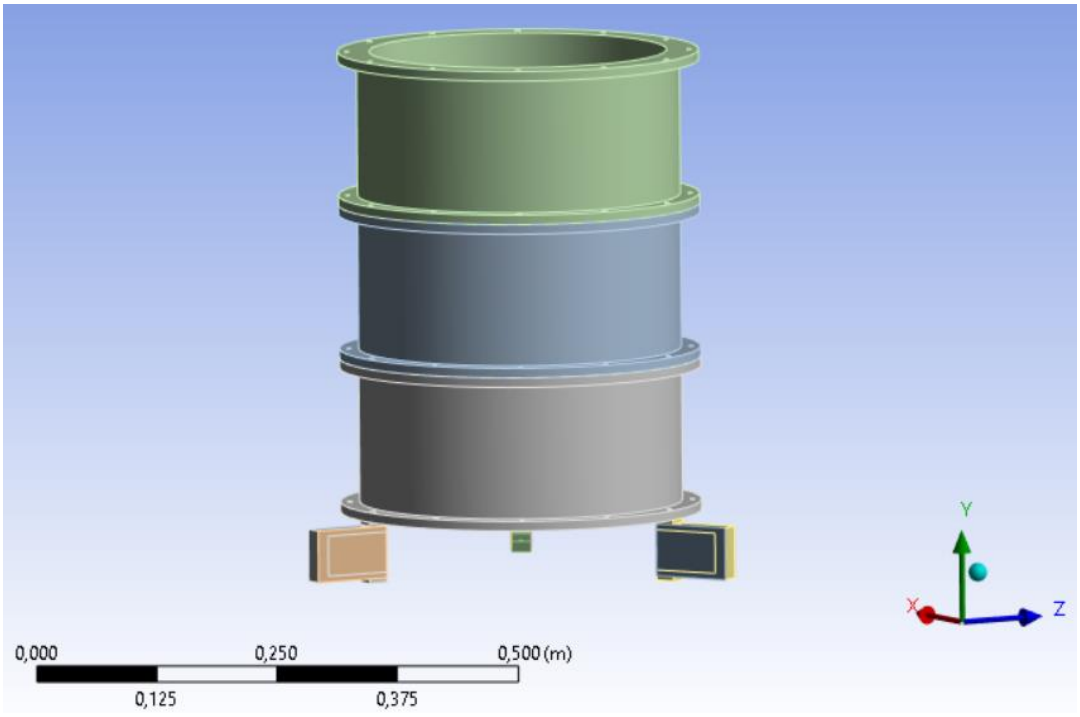

Figure 5.1 General View of Previous Triple Test Configuration

Previously designed triple test structure is shown in Figure 5.1, There are three VEM layered metal vibration isolators at the base. Moreover, payload is attached to end of the isolators. Payload is approximately 60 kg made up of steel. Material of metal isolators is Al6061-T6. VEM layers consist of 3M-ISD112 polymer and surrounded by aluminum constraining layers. The material properties of the ISD112 is shown in

Figure 5.2. S-N curve of a material is created with the averaged values of typical polymers [30]. In the coordinate system, y refers to axial direction and the others refer to lateral direction.

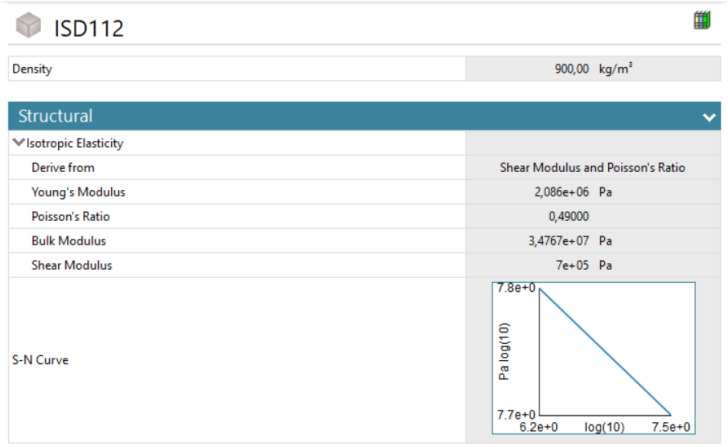

Figure 5.2 Material Properties of ISD112 Polymer

In Figure 5.3, meshing is shown. The most suitable element size is given to the parts by trial. Tetrahedral elements are used in payload part and quadrilateral elements are used in isolator part.

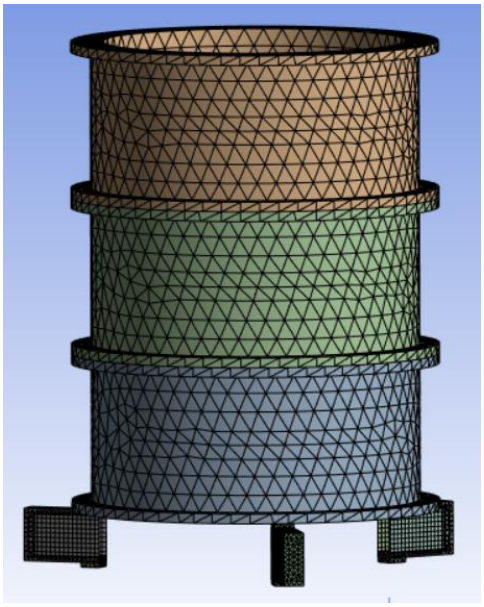

Figure 5.3 Meshing of Triple Test Stucture Assembly

The base of the isolators are fixed as a BC and the other parts are bonded as a contact option. Then, random vibration analysis is performed. One of the system requirement is used as an input which is PSD gRMS input shown in Figure 4.14 for this analysis type. Steinberg method has been used, and Von Mises equivalent stress component has been chosen from the selection menu of ANSYS for life calculations.

In Figure 5.4, equivalent stress results for 3σ is shown for the axial PSD input. It can be said that most critical stresses occur for the VEM layers. The fatigue life in terms of axial input is shown in Figure 5.5 as well. The results looks like system has infinite life by considering axial PSD input.

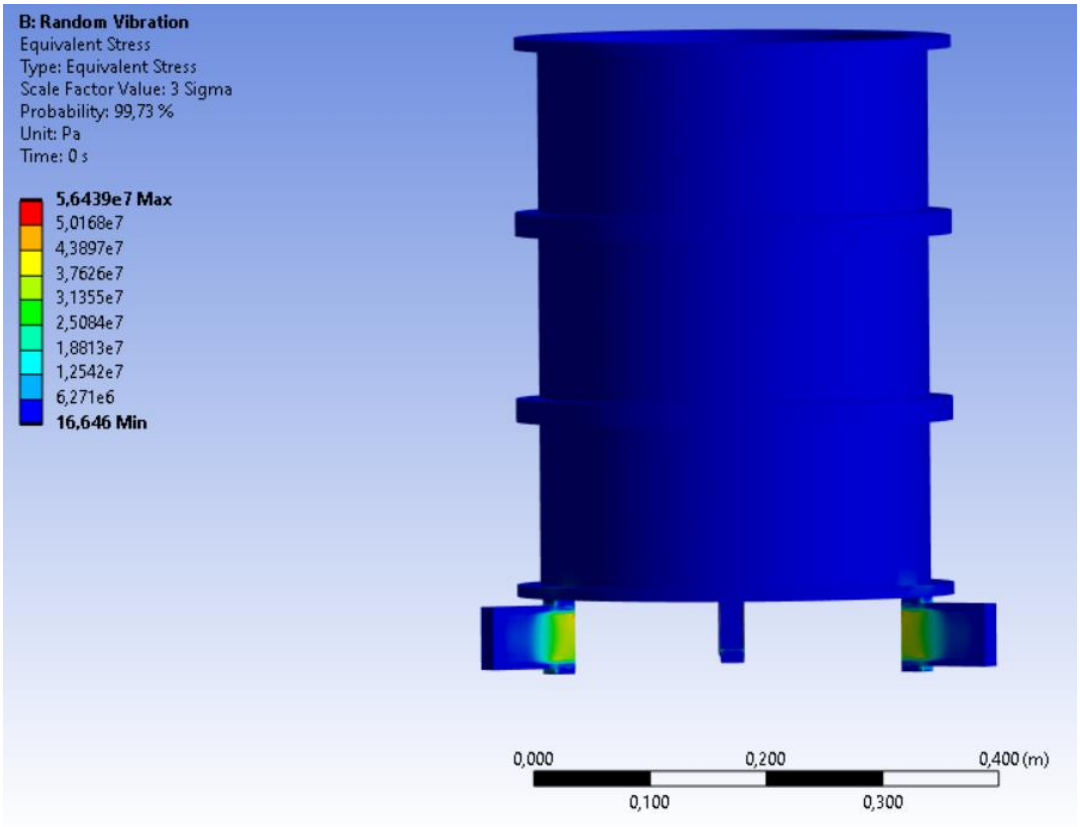

Figure 5.4 Equivalent Stress Results of Triple Test Stucture for Axial PSD Input

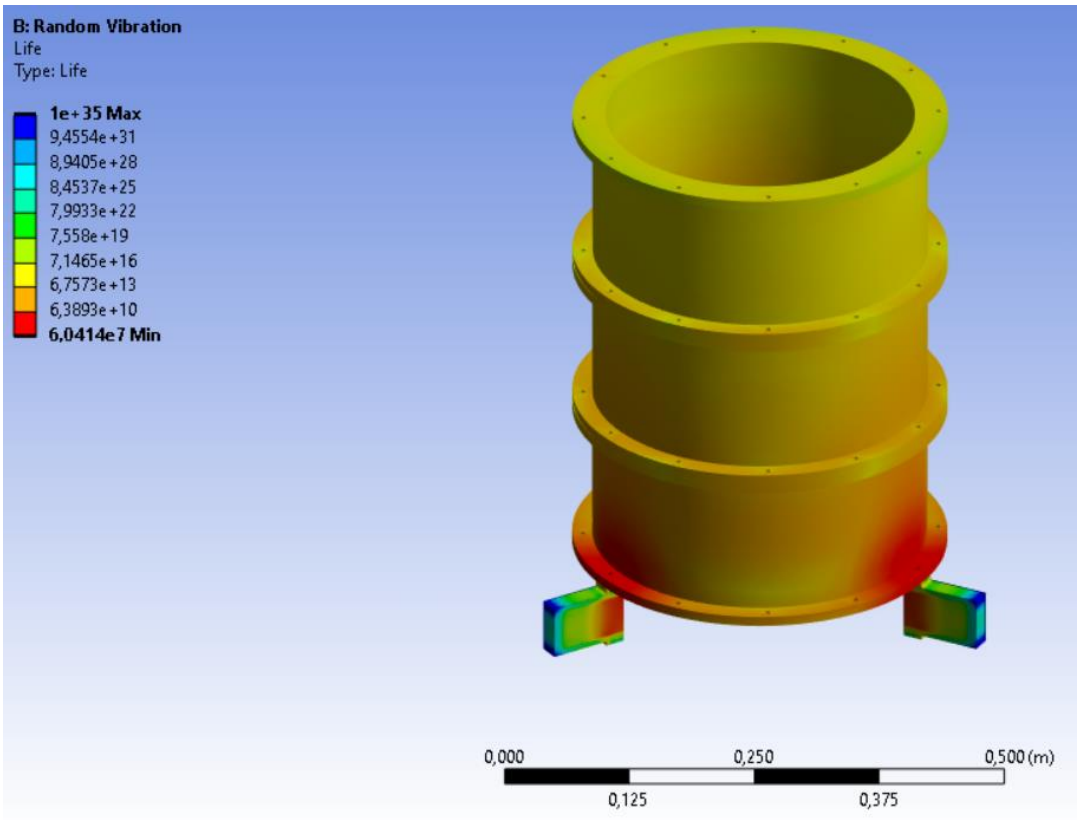

Figure 5.5 Fatigue Life Expactation of Triple Test Stucture for Axial PSD Input

Then, lateral PSD input is given to FEA software. Input PSD is given in the z-direction as a worst case because it stimulates one of the isolator to move in axial direction.

The reults are shown in Figure 5.6 and Figure 5.7. The most critical stress location occurs again on VEM layers. The results looks like system failing from the VEM layer side in 6 hours and 22 minutes by looking the fatigue life results. The predicted S-N curve of the VEM layer is an estimated curve, so the actual life value might be lower or higher.

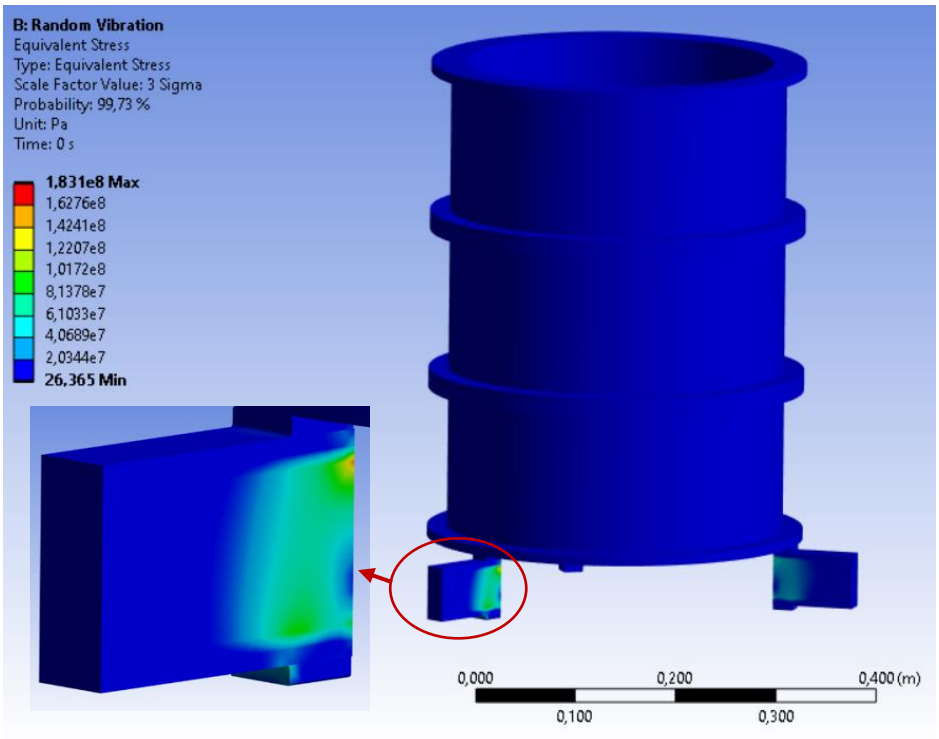

Figure 5.6 Equivalent Stress Results of Triple Test Stucture for Lateral PSD Input

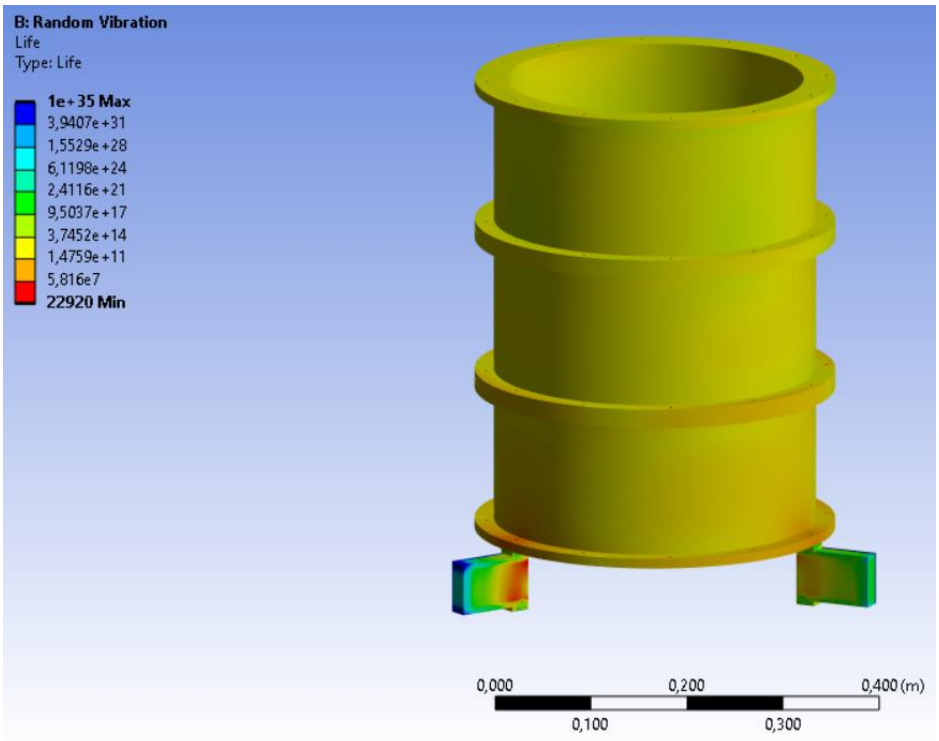

Figure 5.7 Fatigue Life Expactation of Triple Test Stucture for Lateral PSD Input

In order to assess whether a similar behavior occurs in the quadruple test structure, fatigue analysis of the quadruple test configuration has been conducted in lateral direction.

In Figure 5.8, meshing is shown. The most suitable element size is given to the parts by trial. Triangular elements are used in both isolator and payload parts, and quadrilateral elements are used in both VEM layers and adapter jig part.

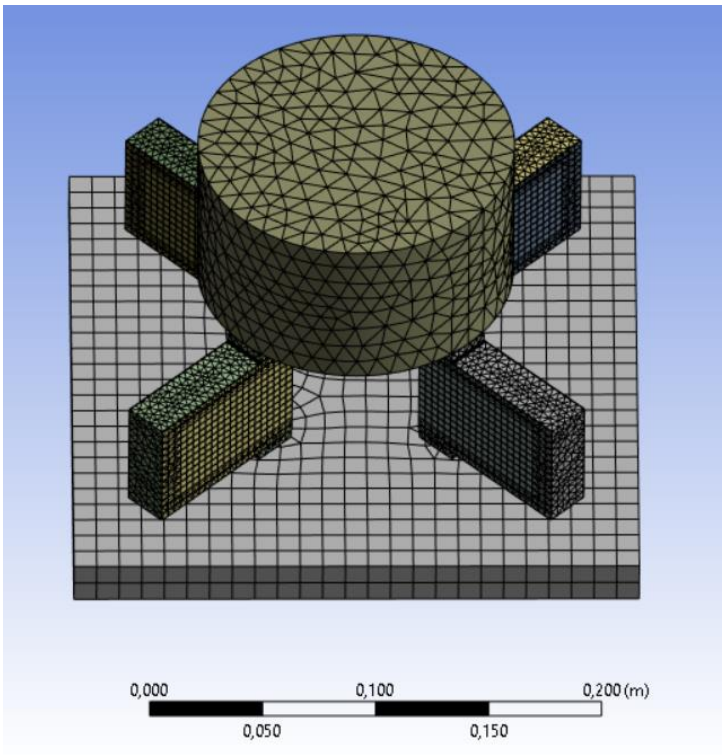

Figure 5.8 Meshing of Quadruple Test Stucture Assembly

The base of the adapter jig is fixed as a BC and the other parts are bonded as a contact option. Then, random vibration analysis is performed. One of the system requirement is used as an input which is PSD gRMS input shown in Figure 4.14 for this analysis type. Steinberg method has been used, and von Mises equivalent stress component has been chosen from the selection menu of ANSYS for life calculations.

In Figure 5.9 and Figure 5.10, the fatigue lifes in terms of lateral input are shown. The results looks like both quadruple test stucture with and without TVA implementation have infinite life by considering lateral PSD input.

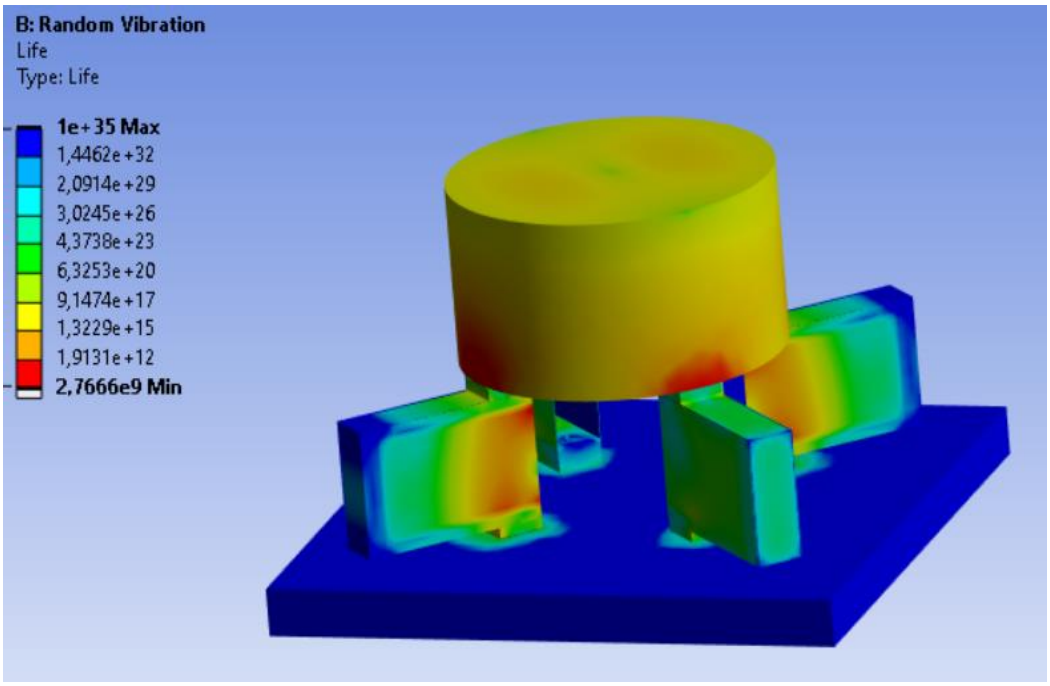

Figure 5.9 Fatigue Life Expactation of Quadruple Test Stucture Without TVAs for Lateral PSD Input

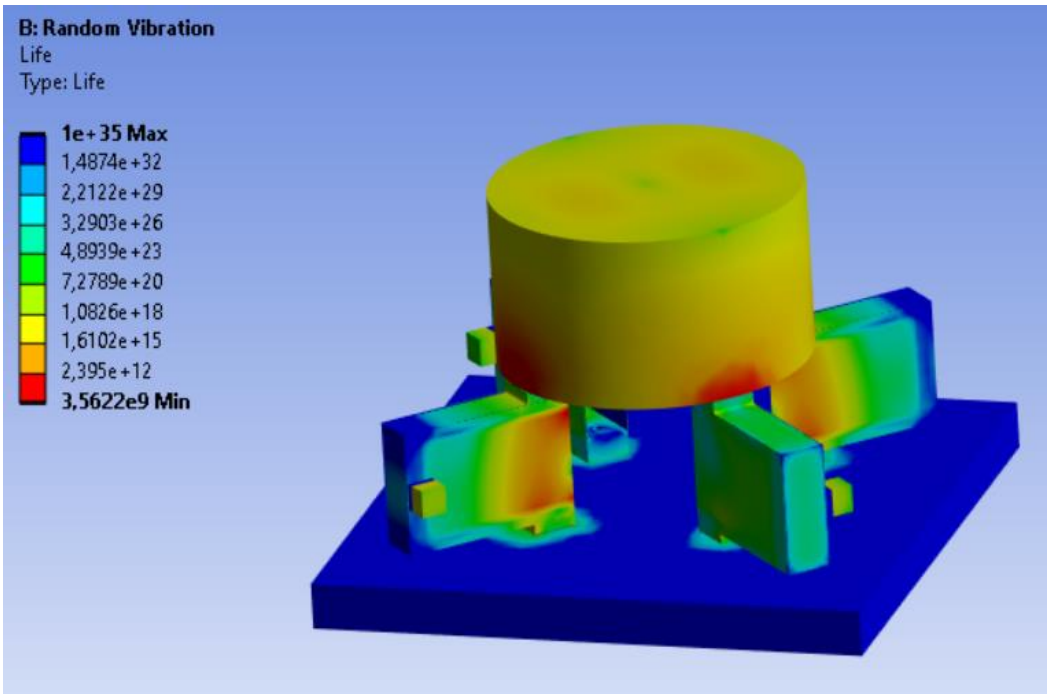

Figure 5.10 Fatigue Life Expactation of Quadruple Test Stucture With TVAs for Lateral PSD Input

The potential areas where metal isolators may experience fractures were identified by removing VEM layers from the triple test structure model, assuming the failure state swhich can be one of viscoelastic material tearing, breaking, or losing its adhesion. The obtained results are shown in Figure 5.11 and Figure 5.12. Possible failure locations of the metal isolators can occur at the interior corners of the part as happened in the previous triple test structure. Therefore, some isolators experience high axial loads although PSD input is given in lateral direction, and it triggers potential for failure in the structure in the case of asymmetric isolator placement.

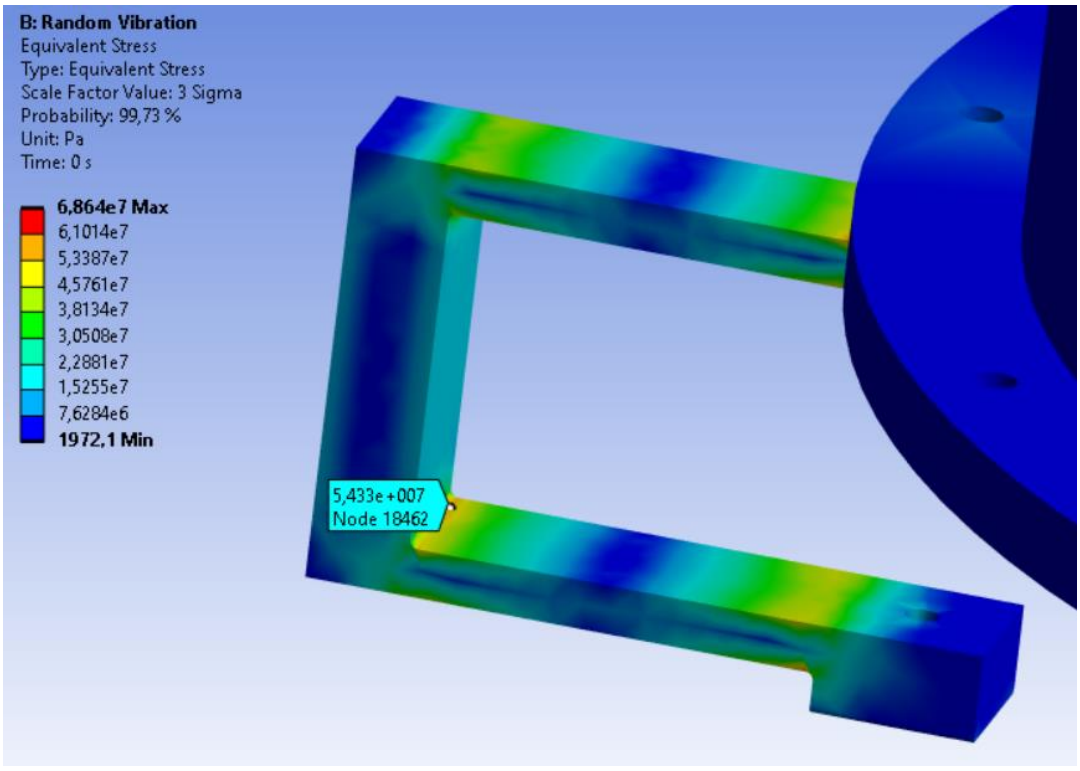

Figure 5.11 Equivalent Stress Results of Isolators Without VEM Layers for Axial PSD Input

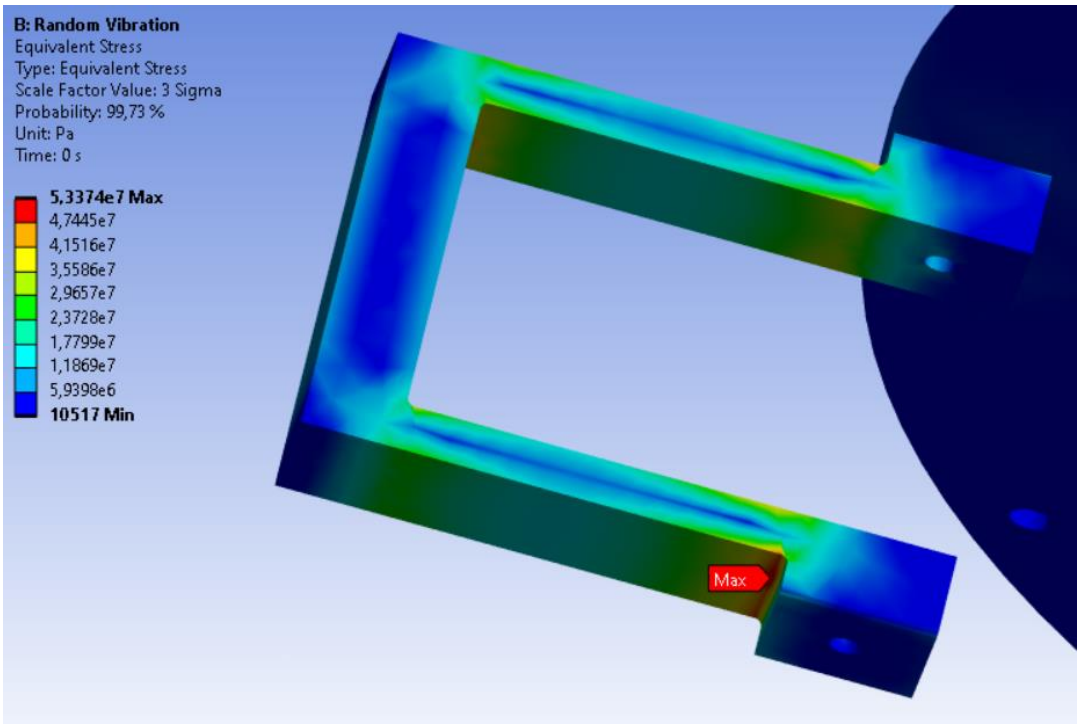

Figure 5.12 Equivalent Stress Results of Isolators Without VEM Layers for Lateral PSD Input

CHAPTER 6

CONCLUSION

Within the scope of this thesis, a design study was conducted to enhance the performance of metal vibration isolators by increasing damping at specific frequencies associated with internal resonance peaks of metal vibration isolators. The feasibility of implementing Tuned Vibration Absorbers (TVA) on previoulsy designed triple test structure was explored to address whether TVA application could be a viable solution. Subsequently, a target mode was identified with the help of vibration isolation system consisting of 60 isolators, and modal shapes were examined to determine suitable locations for TVA implementation. Parametric studies were conducted by adjusting parameters until the desired value was achieved, and further validation was performed through analyses in finite element analsysi softwares, which were later confirmed through experimental tests. In conclusion, the designed quadruple test structure and the previously designed triple test structure were analyzed in terms of fatigue life.

The outcomes of this study contribute to the ongoing efforts to improve the design and performance of metal vibration isolators by incorporating damping techniques and exploring the effectiveness of TVA applications. The combination of parametric studies, FEA analyses, and experimental validations provides a comprehensive understanding of the proposed design modifications and their impact on the overall system dynamics. The thesis includes these results and provides details on this matter in relevant sections. The impact of meshing, accurate definition of material properties, proper integration of input data into the model, and the effect of physical constraints were once again demonstrated in FEA. Moreover, the utilization of an unspecified S-N curve for the material introduced considerable challenges in the process of fatigue life prediction. Hence, it is crucial to precisely define the S-N curve of the material to ensure the reliability and accuracy of fatigue life estimations.

REFERENCES

[1] Johnson, C. D., Wilke, P. S. & Darling, K. R. (2001). Multi-axis whole-spacecraft vibration isolation for small launch vehicles. SPIE Proceedings. https://doi.org/10.1117/12.432699

[2] Yang, J., Sun, S. S., Du, H., Li, W. H., Alici, G. & Deng, H. X. (2014). A novel magnetorheological elastomer isolator with negative changing stiffness for vibration reduction. Smart Materials and Structures, 23 (10), 105023-1-105023-11.

[3] Yan, B., Wang, Z., Ma, H., Bao, H., Wang, K., & Wu, C. (2021). A novel lever-type vibration isolator with eddy current damping. Journal of Sound and Vibration, 494, 115862. https://doi.org/10.1016/j.jsv.2020.115862

[4] Wu, W., Chen, X., & Shan, Y. (2014). Analysis and experiment of a vibration isolator using a novel magnetic spring with negative stiffness. Journal of Sound and Vibration, 333(13), 2958–2970. https://doi.org/10.1016/j.jsv.2014.02.009

[5] Li, H., Wu, Z., & Jiang, T. (2019). A novel quasi-zero stiffness vibration isolator based on hybrid Bistable Composite Laminate. AIAA Scitech 2019 Forum. https://doi.org/10.2514/6.2019-1860

[6] Yilmaz, C., & Kikuchi, N. (2006). Analysis and design of passive band-stop filter-type vibration isolators for low-frequency applications. Journal of Sound and Vibration, 291(3–5), 1004–1028. https://doi.org/10.1016/j.jsv.2005.07.019

[7] Leblouba, M., Altoubat, S., Ekhlasur Rahman, M., & Palani Selvaraj, B. (2015). Elliptical leaf spring shock and vibration mounts with enhanced damping and energy dissipation capabilities using lead spring. Shock and Vibration, 2015, 1–12. https://doi.org/10.1155/2015/482063

[8] Tang, J., Cao, D., Qin, Z., Li, H., & Chen, D. (2018). A VCM-based novel whole-spacecraft vibration isolation device: Simulation and experiment. Journal of Vibroengineering, 20(2), 1035–1050. https://doi.org/10.21595/jve.2017.18494

[9] Kim, G. W., & Kang, J. (2019). The V-shaped band-stop vibration isolator inspired by Middle Ear. Applied Acoustics, 150, 162–168. https://doi.org/10.1016/j.apacoust.2019.02.013

[10] Pierrick, J., Ohayon, R., & Le Bihan, D. (2006). Semi-active control using magnetorheological dampers for payload launch vibration isolation. SPIE Proceedings. https://doi.org/10.1117/12.655924

[11] Johnson, W., & Ruzzene, M. (2018). Challenges and constraints in the application of resonance-based metamaterials for vibration isolation. Health Monitoring of Structural and Biological Systems XII. https://doi.org/10.1117/12.2294919

[12] Park, Y.-H., Kwon, S.-C., Koo, K.-R., & Oh, H.-U. (2021). High damping passive launch vibration isolation system using superelastic SMA with multilayered viscous lamina. Aerospace, 8(8), 201. https://doi.org/10.3390/aerospace8080201

[13] Dunaj, P., Berczyński, S., Miądlicki, K., Irska, I., & Niesterowicz, B. (2020). Increasing damping of thin-walled structures using additively manufactured vibration eliminators. Materials, 13(9), 2125. https://doi.org/10.3390/ma13092125

[14] Wilke, P. S. and Johnson, C. D. (2007). "LOW-PROFILE, MULTI-AXIS, HIGHLY PASSIVELY DAMPED, VIBRATION ISOLATION MOUNT," US 7,249,756 B1.

[15] Turker, C. (2020). *Design and Production Stages of a Vibration Test Fixture,* MSc thesis, Middle East Technical University, Ankara..

[16] Mrabet, E., Ichchou, M. N., & Bouhaddi, N. (2019). Random vibro-acoustic control of internal noise through optimized tuned mass dampers. *Mechanical Systems and Signal Processing*, *130*, 17–40. https://doi.org/10.1016/j.ymssp.2019.04.062

[17] Gardonio, P., & Zilletti, M. (2013). Integrated tuned vibration absorbers: A theoretical study. *The Journal of the Acoustical Society of America*, *134*(5), 3631–3644. https://doi.org/10.1121/1.4824123

[18] Iglesias, A., Aguirre, G., Munoa, J., Dombovari, Z., Laka1, I., & Stepan, G. (2016). Damping of in-process measuring system through variable stiffness tunable vibration absorber. https://past.isma-isaac.be/downloads/isma2016/papers/isma2016_0703.pdf

[19] Jeong, U. (2020). Application of adaptive tuned magneto-rheological elastomer for vibration reduction of a plate by a variable-unbalance excitation. *Applied Sciences*, *10*(11), 3934. https://doi.org/10.3390/app10113934

[20] Rubio, L., Loya, J. A., Miguélez, M. H., & Fernández-Sáez, J. (2013). Optimization of passive vibration absorbers to reduce chatter in boring. *Mechanical Systems and Signal Processing*, *41*(1–2), 691–704. https://doi.org/10.1016/j.ymssp.2013.07.019

[21] Aliakbari, A., Moraru, G., Veron, P., & Groll, Y. (2021). The effect of a polymer-based tuned mass damper on the vibration characteristics of an

anti-vibration boring bar. *Procedia CIRP*, *103*, 200–206. https://doi.org/10.1016/j.procir.2021.10.032

[22] Hua, Y., Wong, W., & Cheng, L. (2018). Optimal design of a beam-based dynamic vibration absorber using fixed-points theory. *Journal of Sound and Vibration*, *421*, 111–131. https://doi.org/10.1016/j.jsv.2018.01.058

[23] Eldoğan, Y., & Cigeroglu, E. (2013). Vibration fatigue analysis of a cantilever beam using different fatigue theories. Topics in Modal Analysis, Volume 7, 471–478. https://doi.org/10.1007/978-1-4614-6585-0_45

[24] Customer Training Material Introduction to ANSYS NCode DesignLife (2012). Ansys Inc. PA, USA.

[25] Miner, M. A. (1945). "Cumulative Damage in Fatigue," J. of Appl. Mech. Trans ASME, pp. 159 164.

[26] Karaman, B. (2018). *Vibration Isolation System For Space Launch Vehicles*, MSc thesis, Middle East Technical University, Ankara..

[27] 3MTM viscoelastic damping polymer 112series. (n.d.). https://multimedia.3m.com/mws/media/828134O/3m-viscoelastic-damping-polymer-112-series.pdf?fn=Viscoelastic%2520Damping%2520Polymers%252011

[28] Jones, D. I. G. (2001). Handbook of viscoealstic vibration damping. NewYork: Wiely

[29] "Minotaur I User's Guide 2.1," 2006.

[30] Zorko, D., Demšar, I., & Tavčar, J. (2021). An investigation on the potential of bio-based polymers for use in polymer gear transmissions. *Polymer Testing*, *93*, 106994. https://doi.org/10.1016/j.polymertesting.2020.106994